

Aus dem Institut für Neuropathologie und Prionforschung
der Ludwig-Maximilians-Universität München
Vorstand: Prof. Dr. med. Dr. h. c. H. A. Kretzschmar

The role of the transcription factor BARHL1 in medulloblastoma

Dissertation
zum Erwerb des Doktorgrades der Medizin
an der Medizinischen Fakultät der
Ludwig-Maximilians-Universität zu München

vorgelegt von
Julia Elisabeth Pöschl

aus
Kösching

Jahr
2011

Mit Genehmigung der Medizinischen Fakultät
der Universität München

Berichterstatter:	PD Dr. Ulrich Schüller
Mitberichterstatter:	PD Dr. Ennes A. Auerswald apl. Prof. Dr. Joachim-Ulrich Walther apl. Prof. Dr. Hans Gustav Klobeck
Dekan:	Prof. Dr. med. Dr. h.c. M. Reiser, FACR, FRCR
Tag der mündlichen Prüfung:	01.12.2011

Major parts of this work have been published as:

Expression of *BARHL1* in medulloblastoma is associated with prolonged survival in mice and humans

J Pöschl, A Lorenz, W Hartmann, A O von Bueren, M Kool, S Li, A Peraud, J-C Tonn, J Herms, M Xiang, S Rutkowski, H A Kretzschmar and U Schüller

Oncogene 30, 4721-4730 (24 November 2011) | doi:10.1038/onc.2011.173.

Epub 2011 May 23

(<http://www.nature.com/onc/journal/v30/n47/full/onc2011173a.html>)

Contents

1. Introduction.....	4
1.1. The medulloblastoma.....	4
1.2. The transcription factor BARHL1.....	6
1.3. Aim of this study.....	6
2. Material and Methods.....	8
2.1. Patients and tumor samples.....	8
2.2. Transgenic mice.....	10
2.3. DNA and RNA extraction, real-time RT-PCR.....	13
2.4. Histology, in situ hybridization and immunohistochemistry.....	17
2.5. Western Blot analysis.....	18
2.6. Statistical Analysis.....	19
3. Results.....	20
3.1. <i>BARHL1</i> expression in human medulloblastomas.....	20
3.2. <i>Barhl1</i> expression in Shh-induced mouse medulloblastoma and its cerebellar precursor cells.....	24
3.3. Function of <i>Barhl1</i> <i>in vivo</i>	26
3.3.1. Deletion of <i>Barhl1</i> in mouse medulloblastoma.....	26
3.3.2. Immunohistochemical characterization of mouse medulloblastoma.....	28
3.4. BARHL1 expression in human medulloblastomas and patients' survival.....	31
4. Discussion.....	35
5. Summary.....	38
5.1. Summary.....	38
5.2. Zusammenfassung.....	39
6. References.....	40
7. Acknowledgements.....	44
8. Appendix: Curriculum vitae.....	45

1. Introduction

1.1. The medulloblastoma

Medulloblastoma is a primitive neuroectodermal tumour (PNET) arising in the posterior fossa (Kleihues and Sobin, 2000). It is the most frequent malignant brain tumor in childhood and accounts for approximately 20 percent of all primary tumors of the central nervous system in children and adolescents (Gjerris *et al.*, 1998). The overall incidence rate is about 4.5 cases per million child years in the United Kingdom (Alston *et al.*, 2003; Thorne *et al.*, 1994) with similar incidence rates in other countries (Gjerris *et al.*, 1998). The highest incidence is found in children between five and nine years of age (Alston *et al.*, 2003). Being a tumor of the posterior fossa, medulloblastoma often presents with ataxia and ophthalmologic signs and with symptoms of increased intracranial pressure, for example headaches and vomiting (Alston *et al.*, 2003). Although centralized and evidence based treatment protocols have significantly improved the outcome of patients, still up to 30% of the children succumb to their disease within 5 years (Gilbertson, 2004). Currently, optimal treatment of medulloblastoma is a combination of maximal surgical resection, radiation therapy of both the tumor site and the craniospinal axis, and systemic chemotherapy (Taylor *et al.*, 2003; Tarbell *et al.*, 1991; Hughes *et al.*, 1988; Evans *et al.*, 1990; Kortmann *et al.*, 2000; Tait *et al.*, 1990). Major issues that challenge patients and physicians are the strong tendency of this cancer to metastasize along the cerebrospinal axis together with the fact that specific treatment options based on a tumor's molecular background are still lacking. As a consequence, the necessarily aggressive treatment can lead to severe side effects including neurocognitive impairment, hearing loss, endocrine abnormalities and secondary cancers (Ris *et al.*, 2001; Rademaker-Lakhai *et al.*, 2006; Packer *et al.*, 2006; Laughton *et al.*, 2008; Xu *et al.*, 2004). In this context, it was essential to find that many familial and sporadic medulloblastomas are caused by a constitutive activation of either the Sonic hedgehog (Shh) or the Wnt/beta-catenin signaling pathway, and researchers are now trying to establish well-tolerated drugs that may inhibit these pathways (Crawford *et al.*, 2007; Scales and de Sauvage, 2009). Apart from these two well-defined groups of medulloblastomas, more recent studies identified

additional groups that are distinguishable by array-based expression analysis (Kool *et al.*, 2008; Cho *et al.* 2011; Northcott *et al.* 2011, Figure 1).

Medulloblastoma type	A	B	C	D	E
Molecular characteristics	WNT / TGF signaling β-catenin mutations	SHH signaling PTCH1 mutations			
	NOTCH / PDGF signaling				
	Increased protein biosynthesis / cell cycle				Increased protein biosynthesis / cell cycle
			Neuronal differentiation		
				Photoreceptor differentiation	
Genetic characteristics	Loss of chrom 6	Loss of chrom 9q	Loss of chrom X, gain of chrom 18		
			Loss of chrom 8 and 17p, gain of chrom 17q		
Clinical characteristics	Classic histology	Desmoplastic histology	Mainly classic histology		
			Metastasis		
	Older children	Young children + adults	Children	Children	Young children

Figure 1 (Kool *et al.*, 2008): Kool and colleagues analyzed expression data of 62 medulloblastoma samples and identified 5 distinct clusters of medulloblastomas, indicated as A, B, C, D, and E. Schematic overview from Kool *et al.* 2008 with molecular, genetic, and clinical characteristics.

Nevertheless, the diagnosis of medulloblastomas is still established according to the WHO (World Health Organization) criteria for the classification of central nervous system tumors, and these criteria are solely based on standard histology and immunohistochemistry (Louis *et al.*, 2007). Interestingly, the desmoplastic and the rare extensively nodular variant of medulloblastomas, which typically show tumor nodules surrounded by very cell-dense areas containing reticulin fibers, largely overlap with tumors that are molecularly characterized by constitutive Shh signaling. All other molecular subgroups of medulloblastomas are mainly covered by histologically classic

medulloblastomas (Kool *et al.*, 2008; Northcott *et al.* 2011, see Figure 1). Medulloblastomas of all groups display a neuronal protein expression signature and they are believed to arise from neuronal precursor cells. It is still unclear whether different subtypes of medulloblastomas may arise from different precursor populations, and indeed, recent advances have now proven in vivo that brainstem precursors may give rise to Wnt-associated medulloblastomas (Gibson *et al.* 2010), whereas granule neuron precursors are susceptible to develop Shh-associated medulloblastomas (Schüller *et al.*, 2008). The mechanisms that control proliferation, differentiation and migration of these precursors have therefore been of particular interest to cancer researches, and the understanding of these mechanisms is considered crucial for the development of novel treatment strategies.

1.2. The transcription factor BARHL1

One of the transcription factors that regulate both the survival and the migration of cerebellar granule neuron precursors is the homeobox gene *Barhl1* (Li *et al.*, 2004). *Barhl1* is a mammalian homolog of the *Drosophila BarH1* and *BarH2* genes, which encode homeodomain proteins that are primarily expressed in migrating neurons settling in specific domains within the diencephalon, rhombencephalon and spinal cord (Bulfone *et al.*, 2000). Loss of *Barhl1* function causes attenuated cerebellar foliation, defective radial migration and impaired survival of cerebellar granule neurons (Li *et al.*, 2004). Interestingly, *BARHL1* was also identified to be expressed in medulloblastomas (Yokota *et al.*, 1996), but its functional significance for tumor development and progression has not yet been investigated.

1.3. Aim of this study

The aim of this study is to define the role of *BARHL1* in medulloblastoma. Several intentions are pursued: (1) *BARHL1* expression levels in cerebella and in medulloblastomas of mice and humans are determined. (2) A mouse model for Shh-induced medulloblastoma is used to examine the function of *Barhl1* *in*

vivo. (3) The prognostic significance of *BARHL1* expression levels in human and murine medulloblastomas is investigated by evaluating the overall survival of mice and humans.

2. Material and Methods

2.1. Patients and tumor samples

A total of 44 surgical tumor samples from patients with medulloblastoma were analyzed. Patients included 25 males and 19 females. They were treated in the University Hospitals of Munich, Göttingen, Bremen, Hannover and Münster (all Germany). The majority of patients were enrolled in the German Society of Pediatric Hematology and Oncology multicenter treatment studies for pediatric malignant brain tumors (HIT). The average age was 11.0 years, and the median age was 7.0 years, ranging from 0.6 to 39.7 years. The follow up in survivors ranged from 1.1 to 145.2 months with an average of 55.8 months and a median of 46.0 months. 13 patients succumbed to their disease, and 31 were alive as of September 1, 2010. The study included 29 medulloblastomas of classic histology, 11 medulloblastomas of desmoplastic histology and 4 medulloblastomas with extensive nodularity. An overview on clinical data and histology is given in Table 1. Tumor diagnosis was established by standard light-microscopic evaluation of H&E sections and silver stains. Diagnoses were made independently by at least two neuropathologists based on the criteria of the latest WHO brain tumor classification (Louis *et al.*, 2007). For gene copy number analysis, tumor tissues obtained from six glioblastoma multiforme were included as controls. Autopsy material of normal cerebella was obtained from patients, who gave their informed consent. Patient age ranged between 18 and 67 years for the adult cerebella and between 22 weeks of gestation and 6 months for the developing cerebella. None of these patients died from a central nervous system disorder or showed neuropathological abnormalities on histological examination. All tissue samples were either immediately fixed in formaldehyde and embedded in paraffin or snap frozen and stored at -80°C until use.

Table 1: Summary of tumor pathology and clinical data in examined medulloblastoma cases. NED: no evidence of disease. DOD: death of disease.

Sample number	MB subtype	Sex	Age [years]	Follow up [months]	State	Relative <i>BARHL1</i> mRNA expression
1	classic	f	0.6	12.7	DOD	37.87
2	classic	m	2.4	21.0	DOD	23.13
3	classic	f	3.6	21.1	DOD	5.48
4	classic	f	3.7	5.4	NED	133.63
5	classic	f	3.8	47.1	NED	9.02
6	classic	m	4.1	35.4	NED	0.01
7	classic	m	4.9	75.7	DOD	16.69
8	classic	m	5.4	135.6	NED	47.93
9	classic	f	5.5	28.3	DOD	26.14
10	classic	m	5.5	137.5	NED	60.78
11	classic	m	5.9	1.1	NED	44.54
12	classic	f	6.1	145.2	NED	1.92
13	classic	m	6.2	22.2	DOD	2.96
14	classic	m	6.7	33.4	NED	366.14
15	classic	m	7.0	113.2	NED	2.07
16	classic	m	7.0	142.8	NED	2.08
17	classic	m	7.9	24.1	DOD	0.52
18	classic	m	8.5	36.5	DOD	26.54
19	classic	m	8.8	8.8	NED	367.04
20	classic	m	9.3	50.3	NED	56.40
21	classic	m	9.9	79	NED	0.49
22	classic	m	10.6	23.7	NED	1.07
23	classic	m	16.5	18.3	NED	1.07
24	classic	m	22.3	35.3	NED	2.68
25	classic	f	23.6	80.8	NED	54.73
26	classic	f	25.5	133.7	NED	86.59
27	classic	f	29.3	19.5	NED	5.84
28	classic	m	37.5	4.8	DOD	35.06
29	classic	m	39.7	24.4	DOD	2.15
30	desmoplastic	f	1.6	66.9	NED	2.92
31	desmoplastic	f	2.2	128.0	NED	62.27
32	desmoplastic	m	2.5	7.0	DOD	0.08
33	desmoplastic	m	7.5	14.2	DOD	3.56
34	desmoplastic	m	10.0	101.4	NED	78.99
35	desmoplastic	f	14.3	62.7	DOD	778.79
36	desmoplastic	m	22.8	47.3	NED	8.26
37	desmoplastic	f	25.5	75.5	NED	0.46
38	desmoplastic	f	26.5	46.0	NED	54.33
39	desmoplastic	f	30.5	46.4	NED	4.72
40	desmoplastic	f	30.7	17.7	NED	12.91
41	extensively nodular	f	0.7	107.3	NED	0.15
42	extensively nodular	f	2.2	175.6	NED	3.27
43	extensively nodular	m	2.7	5.6	NED	1.97
44	extensively nodular	f	2.9	78.4	NED	0.18

2.2. Transgenic mice

Barhl1^{-/-} mice

Barhl1^{-/-} mice have been obtained from Dr. Shengguo Li and Prof. Dr. Mengqing Xiang (University of Medicine and Dentistry of New Jersey). To knock out *Barhl1*, the three *Barhl1*-coding exons were replaced with *lacZ* marker DNA and a *PGK-Neo* cassette flanked by two *loxP* sites (Li *et al.*, 2002, see Figure 2). Primers for wild type *Barhl1* were: *Barhl1* WT Fw, 5'-GCTGAGTCCACGCTCAGAGAGCAG -3'; *Barhl1* WT Rv, 5'-CTCAGAGTCTGATGAAGCGCTGCTG -3' (Li *et al.*, 2002). *Barhl1* knockout was detected with the following primers: *Barhl1* Fw, 5'-CCCATTCTCCTGACACTC -3'; *LacZ* Rv, 5'-GACAGTATCGGCCT-CAGGAA -3' (see Figure 2).

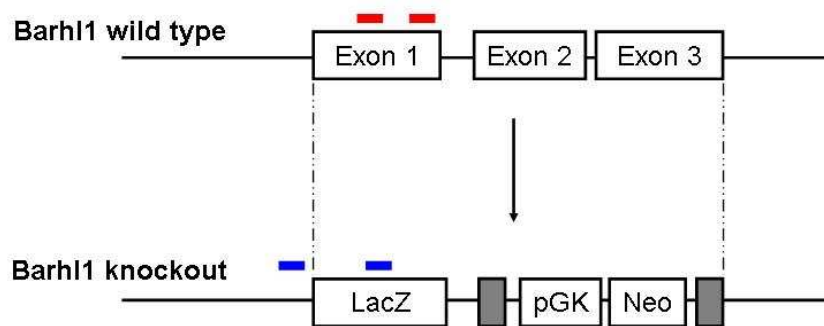


Figure 2: Schematic structure of the *Barhl1* knockout allele generated by Li and colleagues. The three *Barhl1*-coding exons were replaced with *lacZ* marker DNA and a *PGK-Neo* cassette flanked by two *loxP* sites (grey boxes). The red bars represent the primers to detect the *Barhl1* wild type genotype, the blue bars represent the primers to detect the *Barhl1* knockout genotype.

Math1-cre mice

Math1-cre transgenic mice carry the bacteriophage P1 cre recombinase under control of a 1.4-kb upstream *Math1* enhancer element (Heine and Rowitch, 2009; Schüller *et al.*, 2007; Matei *et al.*, 2005). As a consequence, cre is produced specifically in cerebellar granule cell precursor cells (Schüller *et al.*,

2007). Internal cre primers were used to detect the *Math1-cre* allele: *cre Fw*, 5'-TCCGGGCTGCCACGACCAA -3'; *cre Rv* 5'-GGCGCGGCAACACCATTTT -3' (Heine and Rowitch, 2009).

SmoM2^{Ft/Ft} (Gt(ROSA)26Sor^{tm1(Smo/EYFP)Amc}/J mice

SmoM2^{Ft/Ft} (Gt(ROSA)26Sor^{tm1(Smo/EYFP)Amc}/J (Mao *et al.*, 2006) mice were obtained from Jackson Laboratory (Bar Harbour, ME, USA). In these mice, a floxed neo/4xpA-SmoM2-YFP cassette was inserted into pROSA26PA (Srinivas *et al.*, 2001; Mao *et al.*, 2006, see Figure 3). SmoM2 itself contains a point mutation, defined as W539L, which leads to constitutive activation of Smoothed and consequently to a permanent activation of the Sonic hedgehog pathway (Xie *et al.*, 1998). Primers used to detect *SmoM2* and the wild type allele were as follows: *SmoM2 Fw*, 5'-AAGTTCATCTGCACCACCG -3'; *SmoM2 Rv*, 5'-TCCTTGAAGAAGATGGTGCG -3'; *Smo WT Fw*, 5'-GGAGCGGGAGAAATGGATATG -3'; *Smo WT Rv*, 5'-CGTGATCTGCAACTCCAGTC -3' (Jeong *et al.*, 2004; Soriano, 1999).

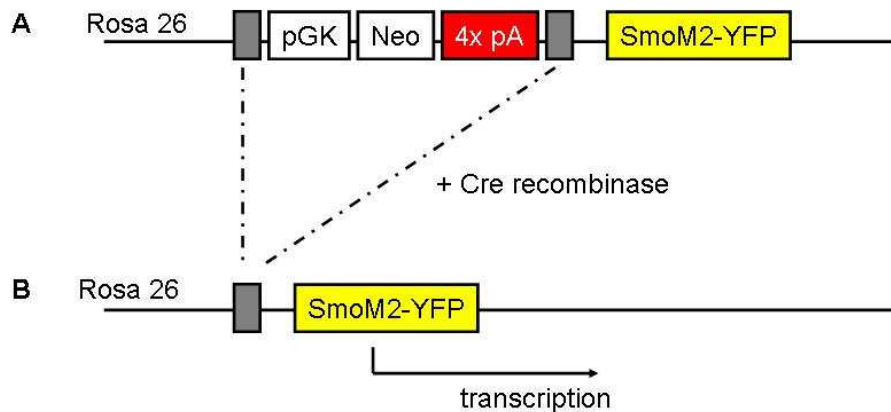


Figure 3: (A) Schematic structure of the *SmoM2^{Ft/Ft} (Gt(ROSA)26Sor^{tm1(Smo/EYFP)Amc}/J* mouse model created by Mao and colleagues. A fused gene composed of SmoM2 and yellow fluorescent protein (YFP) was targeted into the Rosa26 locus. Upstream, a polyadenylation stop sequence cassette (4x pA) was inserted to prevent expression of the mutant *Smoothed*. (B) If cre recombinase is present, the LoxP-flanked polyadenylation stop sequence is removed and the mutant *Smoothed* will be expressed leading to autonomous activation of the Sonic hedgehog pathway.

Barhl1^{-/-} mice, *Math1-cre* mice and *SmoM2*^{F/FI} (*Gt(ROSA)26Sor*^{tm1(Smo/EYFP)Amc}/J mice were crossed to produce *Math1-cre:SmoM2*^{F/+}, *Barhl1*^{+/-}*Math1-cre:SmoM2*^{F/+} and *Barhl1*^{-/-}*Math1-cre:SmoM2*^{F/+} mice. To exclude influences of the genetic background, the mice were crossed in a manner that all examined genotypes (*Math1-cre:SmoM2*^{F/+}, *Barhl1*^{+/-}*Math1-cre:SmoM2*^{F/+} and *Barhl1*^{-/-}*Math1-cre:SmoM2*^{F/+} mice) were produced in one litter. Figure 4 shows a schematic overview of breeding. Genotyping for all mice was done by PCR analysis using genomic DNA from mouse tail biopsies. Each tail biopsy was lysed for 2 hours at 55°C using 300 µl lysis buffer (containing 100 mM Tris pH 8.5, 5 mM EDTA pH 8.0, 0.2% SDS (filtered) and 200 mM NaCl) and 10 µl of Proteinase K. 300 µl of Phenol:Chloroform:Isoamyl Alcohol (25:24:1, v/v; Invitrogen) was added and the sample was mixed for 5 minutes. Centrifugation at room temperature was done for 15 minutes with 13000 x g. The top layer was extracted (about 200 µl) and 50 µl of 3 M sodium acetate (pH 5.2) and 1 ml of cold 95% ethanol were added. After mixing, centrifugation was done at 4°C for 10 minutes with 13000 x g. The liquid was discarded and the remaining pellet was washed with 800 µl 70% ethanol. After another centrifugation at 4°C for 10 minutes with 13000 x g all liquid was removed and the pellet containing the DNA was dissolved in 100 µl DEPC water and stored at 4°C. Tumor-prone mice carrying both the *Math1-cre* and the *SmoM2* allele (see Figure 4) were monitored twice daily for signs of neurological symptoms or general weakness.

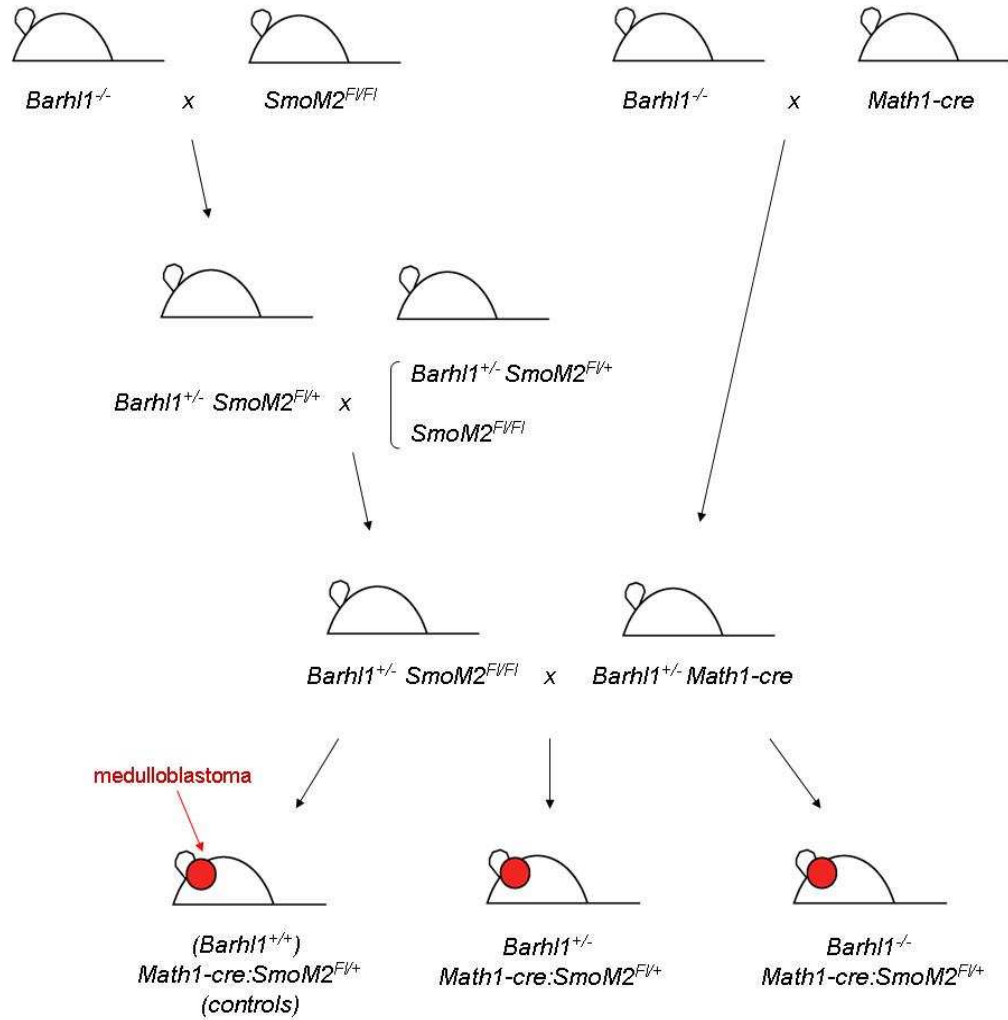


Figure 4: Principles of breeding

2.3. DNA and RNA extraction, Real-time RT-PCR

For DNA and RNA extraction paraffin-embedded tissues containing at least 90% tumor material, as confirmed by H&E sections, were used. For snap-frozen tissues instantaneous sections were performed to assure a tumor fraction of at least 90%. DNA for real-time RT-PCR analysis was extracted from formalin-fixed paraffin-embedded tissues using the QIAamp DNA FFPE Tissue Kit (Qiagen). Total RNA was extracted from snap-frozen tissues using TRizol[®] reagent (Invitrogen). 20 - 30 10 μ m slices of snap-frozen tissue were carefully

mixed with 750 μ l Trizol and incubated at room temperature for 5 minutes. 150 μ l chloroform was added and the composite was mixed and incubated at room temperature for 3 minutes. Centrifugation was done at 4°C for 15 minutes with 14000 x g. The top layer containing RNA and chloroform was extracted (about 300 μ l) and 375 μ l isopropanol were added to precipitate the RNA. After mixing, centrifugation was done at 4°C for 10 minutes with 14000 x g. The liquid was discarded and the pellet was washed with 750 μ l 75% ethanol. Another centrifugation was done at 4°C for 5 minutes with 7500 x g. The ethanol was removed and the remaining RNA was dissolved in 24 μ l DEPC water and stored at -80°C. Total RNA from paraffin-embedded tissues was obtained using the RNeasy FFPE Kit (Qiagen). Total RNA was treated with RNase-Free DNase (Promega). Therefore, 8 μ l RNA (in DEPC water), 1 μ l RQ1 RNase-Free DNase 10x Reaction Buffer and 1 u/ μ g RNA of RQ1 RNase-Free DNase were mixed and incubated at 37°C for 30 minutes. Then, 1 μ l of DNase Stop solution was added to terminate the reaction. The mixture was incubated at 65°C for 10 minutes to inactivate the DNase. Superscript II reverse transcriptase (Invitrogen) was used to run reverse transcription for human samples. Up to 4 μ g total RNA in up to 8 μ l was used for the reaction. For each reaction 0.5 μ l Oligo (dT)₁₅ primers and 0.5 μ l random hexamers (50 ng/ μ l) were mixed and added to the RNA. 1 μ l of 10 mM dNTP mix was added. If less than 8 μ l of RNA were used, the composite was filled to 10 μ l with DEPC-treated water. The sample was incubated at 65°C for 5 minutes and then cooled on ice for at least 1 minute. 9 μ l of reaction mixture (containing 2 μ l 10X RT buffer, 4 μ l 25 mM MgCl₂, 2 μ l 0.1 M DTT and 1 μ l RNaseOUT Recombinant Ribonuclease Inhibitor (all Invitrogen)) were added to each sample, the composite was mixed carefully and incubated at 25°C for 2 minutes. 1 μ l (50 units) of Superscript II reverse transcriptase (Invitrogen) were added to each sample. The mixture was incubated at 25°C for 5 minutes, at 42°C for 50 minutes and at 70°C for 15 minutes. The samples were stored on ice. After adding 1 μ l of RNase H (Invitrogen), the sample was incubated at 37°C for 20 minutes. Reverse transcription of mouse samples was performed using random hexamers and Transcriptor High Fidelity Reverse Transcriptase (Roche). Up to 4 μ g total RNA were mixed with 1 μ l anchored-oligo(dT)₁₈ Primers (50 pmol/ μ l) and 1 μ l Random Hexamer Primers (600 pmol/ μ l) and PCR-grade water was added to fill the sample volume to 11.4 μ l. The template-primer mixture was denatured by

incubating for 10 minutes at 65°C. For each reaction, 8.6 µl of RT mix (containing 4 µl 5x Transcriptor High Fidelity Reverse Transcriptase Reaction Buffer, 0.5 µl Protector RNase Inhibitor 40 u/µl, 2 µl Deoxynucleotide Mix (10 mM), 1 µl DTT and 1.1 µl Transcriptor High Fidelity Reverse Transcriptase (all Roche)) was added and the reagents were mixed carefully. The sample was incubated at 50°C for 30 minutes, at 85°C for 5 minutes and then placed on ice. For real-time quantitative reverse transcriptase (RT)-PCR, the LightCycler®480 system (Roche), with 96 multiwell-plates, and the SYBR Green detection format was used. SYBR Green I is a DNA double-strand-specific dye that can be detected by its fluorescence when binding to the amplified PCR products. For each reaction, 5 µl of LightCycler®480 SYBR Green I Master Mix (containing FastStart Taq DNA Polymerase and DNA double-strand-specific SYBR Green I dye (Roche)), 1 µl of forward (Fw) Primer and 1 µl of reverse (Rv) Primer were added to 3 µl of cDNA. After incubation at 95°C for 5 minutes, 45 PCR Cycles were performed: 95°C for 10 seconds (Denaturation), 57-60°C for 10 seconds (Annealing according to Primers) and 72°C for 15 seconds (Elongation). After each Elongation step fluorescence of SYBR Green I was detected (real-time PCR). Relative quantification was done by normalizing the target gene with a housekeeper gene. Different reaction rounds were normalized by using a calibrator, a positive sample that was measured in every round. *Beta-2-microglobulin* was used as a housekeeper, as it proved to be highly consistently expressed in medulloblastoma cells (data not shown). All analyses were done in triplicates. Primers were designed using the Primer3 software. Sequences of Primers are shown in table 2.

Table 2: Primers used for real-time RT-PCR

Primer name	Sequence
<i>B2M</i> (cDNA) Fw	5'-TGTCCTTTCAGCAAGGACTGG-3'
<i>B2M</i> (cDNA) Rv	5'-GATGCTGCTTACATGTAT CG-3'
<i>BARHL1</i> (cDNA) Fw	5'-GAGCGGCAGAAGTACCTGAG-3'
<i>BARHL1</i> (cDNA) Rv	5'-AGAAATAAGGCGACGGGAAC-3'
<i>B2M</i> (gDNA) Fw	5'-CAGTAAAGGAGTGGGGGATG-3'
<i>B2M</i> (gDNA) Rv	5'-TTGTGTTGAGGCAGGAAAAA-3'
<i>BARHL1</i> (gDNA) Fw	5'-TTCCATTTTCATCCCATCGT-3'
<i>BARHL1</i> (gDNA) Rv	5'- TCTTCCCTTTCCTTCCTTC-3'
<i>B2m</i> Fw	5'-CCTGGTCTTTCTGGTGCTTG-3'
<i>B2m</i> Rv	5'-TATGTTCCG CTTCCCATTCT-3'
<i>Barhl1</i> Fw	5'-CGCTCAACCTCACCGACA-3'
<i>Barhl1</i> Rv	5'-AGAAATAAGGCGACGGGAAC-3'

For each set of primers postamplification melting curves were analyzed with the LightCycler[®]480 software, and agarose gel electrophoresis was performed to verify the presence of a single amplification product. Efficiency correction for each set of primers was done by creating a standard curve. Measured efficiencies are shown in table 3.

Table 3: Primer efficiencies for real-time RT-PCR

Primer name	Efficiency	Annealing temperature
<i>B2M</i> (cDNA) Primers	2.119	58°C
<i>BARHL1</i> (cDNA) Primers	2.002	60°C
<i>B2M</i> (gDNA) Primers	2.007	57°C
<i>BARHL1</i> (gDNA) Primers	2.067	57°C
<i>B2m</i> Primers	2.025	60°C
<i>Barhl1</i> Primers	1.919	60°C

The calibrator normalized relative ratio was calculated the following way:

$$NR = E_T^{[CpT(C) - CpT(S)]} \times E_H^{[CpH(S) - CpH(C)]}$$

The abbreviation NR represents the normalized ratio, E stands for efficiency, T for target gene, H for housekeeper gene, C stands for calibrator, S for sample, and CpT and CpH are abbreviations for the cycle number at target and housekeeper detection threshold (crossing point), respectively.

2.4. Histology, in situ hybridization and immunohistochemistry

For hematoxylin and eosin (H&E) stainings and for immunohistochemical procedures, brain and tumor tissue was fixed in 4% paraformaldehyde/PBS overnight at 4°C. Tissue for frozen sections was equilibrated in 20% glucose/PBS (pH 7.4) and embedded in OCT. 12 µm parasagittal sections were prepared on Superfrost plus slides (Fisher). Tissue for paraffin wax-embedded sections was dehydrated, embedded and sectioned at 5 µm according to standard protocols. Overall morphology was assessed by staining with H&E. All photomicrographs including those from immunohistochemical experiments were taken digitally using an Olympus Bx50 microscope in combination with the Color view Soft imaging system and Cell software (Olympus). In situ hybridization (ISH) was performed on frozen sections. RNA probe was synthesized by mixing 13 µl DEPC treated water, 1 µl linearized template (1 µg/µl), 2 µl 10x transcription buffer (Roche), 2 µl DIG Label Mix (Roche) and 2 µl RNA polymerase (Roche, 20 u/µl). The composite was incubated at 37°C for 2 hours. 0.5 µl of 0.5 M EDTA (pH 8), 100 µl DEPC-H₂O, 10 µl 8 M LiCl, and 300 µl ethanol were added and the sample was incubated at -20°C for 2 hours. Centrifugation was done for 15 minutes at 13000 x g. The pellet was washed with 1 ml 70% DEPC ethanol. Another centrifugation was done for 10 minutes with 13000 x g. The fluid was removed and the pellet was resuspended at 37°C in 50 µl DEPC treated water. 1 µl RNA probe was mixed with 100 µl hybridization buffer (100 ml containing 50 ml Formamide (50%), 25 ml 20x SSC pH 4.5, 1 ml yeast tRNA (10 mg/ml), 10 mg Heparin (100 µg/ml), 1 ml 100x Denhardt's, 100 µl Tween 20, 100 mg CHAPS (0.1%), 1 ml 0.5 M EDTA (5 mM)

and 22 ml DEPC-H₂O). Brain sections were washed with DEPC-PBS (1 ml DEPC in 1 l PBS), fixed with 4% PFA in PBS at room temperature for 15 minutes and treated with 10 µg/ml proteinase K/PBS at room temperature for 10 minutes. Brain sections were hybridized overnight with labeled RNA probes at 65°C, washed twice in 0.2x SSC pH 4.5, 0.1% Tween 20 at 65°C, washed twice in MBST buffer, pH 7.5, containing 100 mM maleic acid, 150 mM NaCl₂, 2 mM levamisole and 0.1% Tween 20, blocked in MBST with 2% BM blocking agent (Roche) and 20% lamb serum, and incubated with alkaline phosphatase labeled anti-DIG antibodies (Roche, 1:2500 in 2% serum) for 2 hours. Sections were washed and color was visualized using BM purple (Roche). Immunohistochemistry was performed on frozen or formalin-fixed, paraffin-embedded, rehydrated, 4 µm thick sections using the avidin–biotin–peroxidase complex (ABC) method on an automated system (BenchMark[®], Ventana). Primary antibodies against Synaptophysin (DAKO, 1:100), MAP2 (Sigma, 1:40000), Cre (Covance, 1:1500), BARHL1 (Chemicon, 1:200), NeuN (Chemicon, 1:300), Zic (gift from Dr. R. Segal, 1:3000), OLIG2 (Chemicon, 1:1000), Sox2 (Chemicon, 1:1000) and phosphorylated Histone H3 (Cell signaling, 1:200) were diluted in phosphate-buffered saline (PBS) and applied on sections for 30 minutes at 42°C. Cell nuclei were visualized by hematoxylin.

2.5. Western blot analysis

Proteins were extracted from frozen tumor samples. Lysis was performed on ice for 30 minutes in 500 µl of ice-cold lysis buffer containing 50 mmol/L Tris-HCl (pH 8), 120 mmol/L NaCl, 0.5% Nonidet P-40, 1 mmol/L phenylmethyl sulfonyl fluoride (Sigma), 100 U/ml aprotinin (Calbiochem), and 0.1 mol/L NaF. Debris was removed by centrifugation for 20 minutes at 12,000 x g and at 4°C. Proteins were separated by electrophoresis on 4 to 12% Bis-Tris gels (Nu-PAGE, Invitrogen) and blotted onto nitrocellulose. To document equal loading of the gels, Ponceau staining of the membranes was performed. Blocking was performed with 10% nonfat dry milk (Bio-Rad, München, Germany) in Tris-buffered saline containing 0.05% Tween 20 and 20% horse serum for 2 hours at room temperature. Filters were incubated with a Cleaved Caspase-3 (Asp175, Cell Signaling Technology) and a β-actin antibody (clone AC-15, Sigma) as

internal control according to the instructions of the manufacturers (Hartmann *et al.*, 2005). Binding of the primary antibody was detected by a secondary antibody labeled with horseradish peroxidase (Amersham). The filters were developed using enhanced chemiluminescence detection reagents (Amersham, Buckinghamshire, UK).

2.6. Statistical analysis

All obtained results were analyzed using the Prism4 software (Graph Pad). Survival of patients and mice was analyzed using Kaplan-Meier survival curves and the Log-rank test was used to examine the significance of results. P-values <0.05 were considered significant. The unpaired t-test was applied to compare the means of two groups with assumed Gaussian distribution and equal variances. If variances were not equal, as confirmed by the F-test, or Gaussian distribution was not expected, the non parametric Mann-Whitney test for unpaired data was used to compare the medians of two groups. To compare protein expression patterns of *Math1-cre:SmO2^{F/+}*, *Barhl1^{+/-}Math1-cre:SmO2^{F/+}* and *Barhl1^{-/-}Math1-cre:SmO2^{F/+}* mice, at least 3 animals were examined in each group and at least 500 tumor cells were counted in each animal. For pHH3 analysis 1000 tumor cells were counted. The respective histograms illustrate the mean with standard errors (error bars). Correlation of two paired data sets was done with Pearson correlation for Gaussian distributions or else with nonparametric Spearman correlation, with r as correlation coefficient.

3. Results

3.1. *BARHL1* expression in human medulloblastomas

Barhl1 was found to have essential roles for cerebellar granule neuron precursors and for the overall development of the cerebellum (Li *et al.*, 2004). Medulloblastomas derive, at least in part, from these precursor cells, and therefore, the purpose was to investigate whether human medulloblastomas express *BARHL1* and how this would functionally be involved in tumorigenesis. In a first step, *BARHL1* expression in a series of 19 normal tissues and 17 different types of cancer was investigated. Serial analysis of gene expression (SAGE) analysis revealed that *BARHL1* was highly expressed in the cerebellum and even stronger in the medulloblastoma, but only weakly in other types of brain cancer. Several types of normal tissues and tumors outside the central nervous system did not show any significant expression of *BARHL1* (Figure 5).

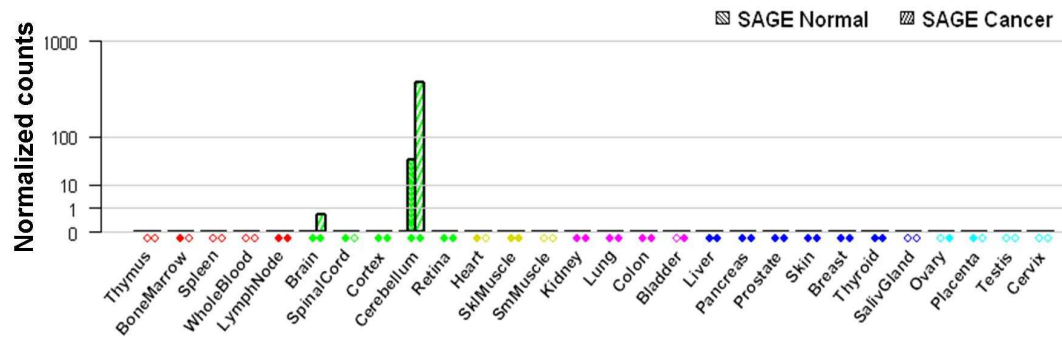


Figure 5: Expression of *BARHL1* in different tissues indicating specificity of high expression in cerebellar tissue and medulloblastoma. Serial analysis of gene expression data for *BARHL1* (SAGE tag: AGCCCGTGAC) is based on data extracted from the Cancer Genome Anatomy project (CGAP) as well as the Genomics institute of the Novartis Research Foundation (GNF) SymAtlas and was obtained from <http://www.genecards.org/index.shtml>. Filled diamonds=insignificant expression after thresholding and normalization. Empty diamonds=no data.

Next, real-time reverse transcriptase (RT)-PCR was used to confirm and extend the expression pattern of *BARHL1* in human cerebellum and in medulloblastoma. As demonstrated in Figure 6, expression of *BARHL1* was about 30-fold higher in the developing cerebellum (n=6) as compared to samples of adult cerebellum (n=8, $p<0.001$). Surgically removed medulloblastoma tissue samples (n=44) were characterized by a more heterogeneous expression pattern with many cases showing strong *BARHL1* expression ($p=0.003$, Figure 6). The median was 7.05 (range, 0.01-778.79) as compared to the median of adult cerebellum samples which was set 1 (Figure 6, Table 1).

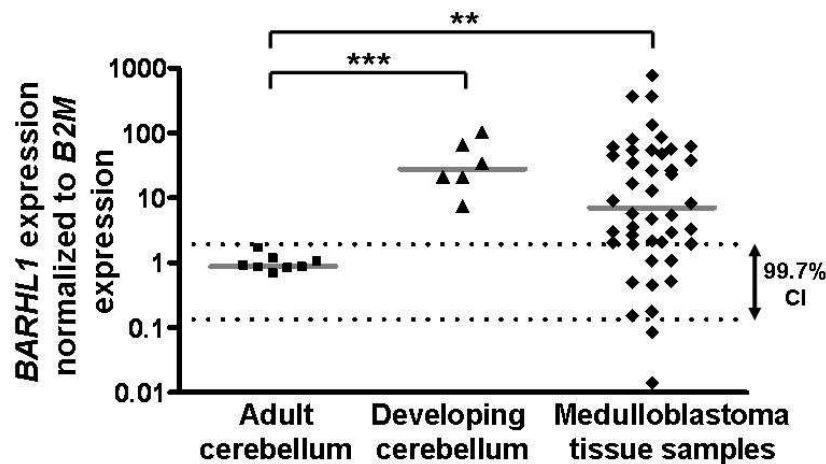


Figure 6: Real-time RT-PCR of adult cerebella (n=8), developing cerebella (n=6) and human medulloblastoma tissue samples (n=44). *BARHL1* expression was normalized to *Beta-2-microglobulin (B2M)* expression. *BARHL1* expression was significantly upregulated in developing cerebella and in medulloblastomas as compared to adult cerebella ($p<0.001$ and $p=0.003$ respectively). Mean of expression in adult cerebella was set 1; dotted lines show mean \pm 3*SD of expression in adult cerebella; solid lines represent median of each group. Two asterisks: $p\leq 0.01$, three asterisks: $p\leq 0.001$.

Patient's age and levels of *BARHL1* expression did not show any significant correlation ($r=0.127$, $p=0.411$, Figure 7).

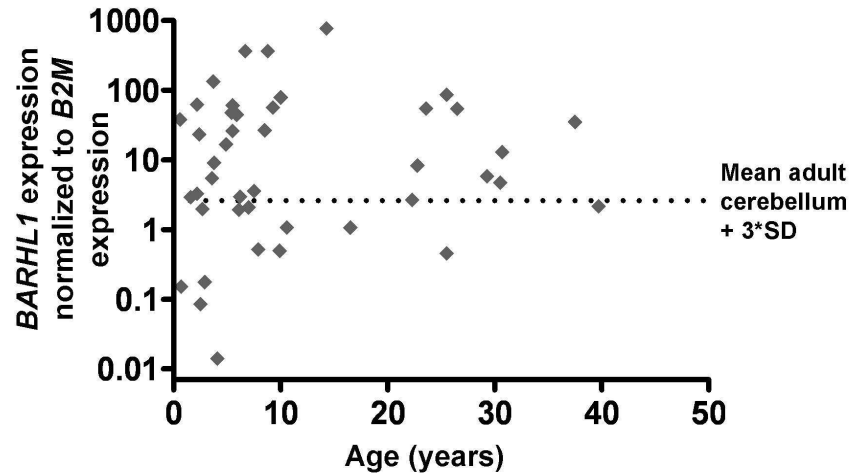


Figure 7: Relative *BARHL1* expression and age distribution of medulloblastoma patients. *BARHL1* overexpression was found in patients between 0.6 and 39.7 years of age. *BARHL1* expression and age did not show any significant correlation ($r=0.127$, $p=0.411$).

The series included 29 classic medulloblastomas and 11 desmoplastic medulloblastomas, but no significant difference with regard to the expression of *BARHL1* in these two histological subtypes could be observed ($p=0.952$, Figure 8).

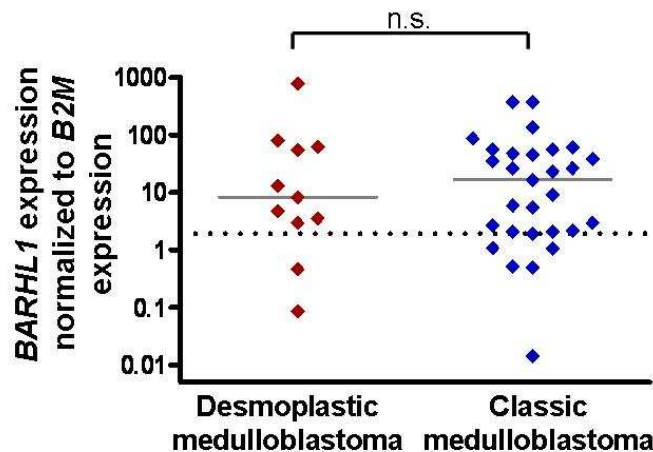


Figure 8: Real-time RT-PCR analysis of *BARHL1* expression in desmoplastic ($n=11$) and classic ($n=29$) medulloblastomas. *BARHL1* overexpression (defined as $>$ mean expression of normal adult cerebellum $+3*SD$, see dotted line) was found in both histological subtypes without statistically significant differences ($p=0.952$). Solid lines: median in each group. CI: confidence interval, n.s.: not significant.

To confirm the RNA expression data, immunohistochemistry on snap-frozen tissues expressing high or low levels of *BARHL1* was performed. Medulloblastoma samples that were shown to highly express *BARHL1* via real-time RT-PCR and that were attributed to the high *BARHL1* group (see Figure 15), exhibited a strong nuclear staining for the transcription factor *BARHL1*, whereas medulloblastoma samples belonging to the low *BARHL1* group (see Figure 15) did not or barely stain for *BARHL1* (Figure 9 A and B).

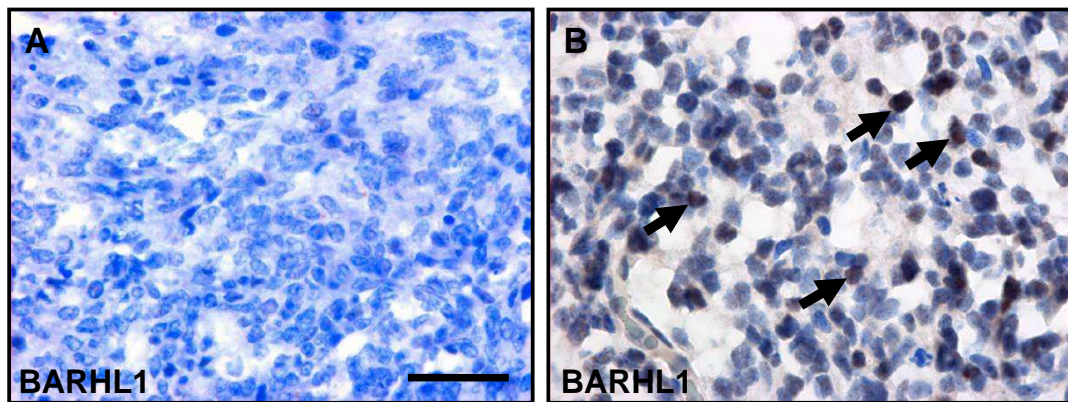


Figure 9: Immunohistochemistry for *BARHL1*. **(A)** Absence of staining for *BARHL1* in medulloblastoma samples exhibiting low levels of *BARHL1* mRNA. **(B)** Arrows point at strong nuclear staining of medulloblastoma cells in medulloblastoma samples that were shown to highly express *BARHL1*. Scale bar is 50 μm .

Finally, quantitative real-time RT-PCR on genomic DNA from medulloblastoma samples ($n=32$) was used to exclude that genomic amplifications were the reason for *BARHL1* overexpression on the mRNA level (Figure 10).

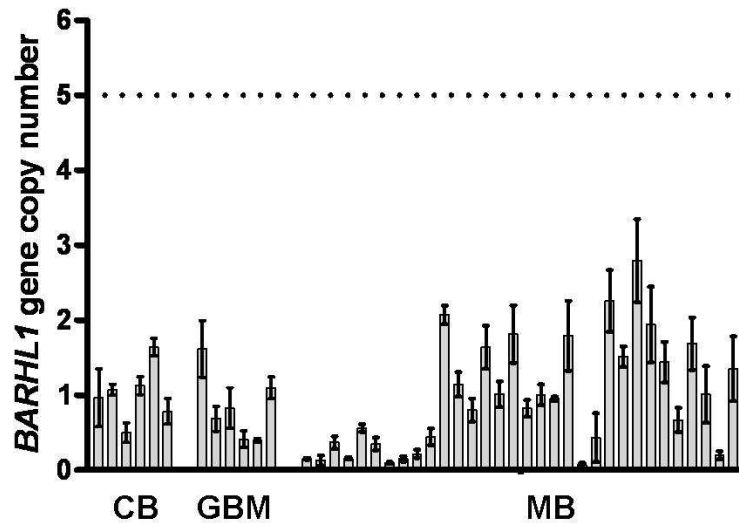


Figure 10: Relative *BARHL1* gene copy number in human medulloblastoma. Real-time PCR analysis was used to quantify the *BARHL1* gene copy number in human medulloblastoma samples. Results were normalized to the *B2M* gene. The mean of relative *BARHL1* gene copy number in adult cerebella was set 1. Amplification was defined as *BARHL1* gene copy number $> 5 \times$ mean of *BARHL1* gene copy number in cerebellar tissue (see dotted line). None of the examined samples were amplified. CB, cerebellum; GBM, glioblastoma; MB, medulloblastoma.

3.2. *Barhl1* expression in Shh-induced mouse medulloblastoma and its cerebellar precursor cells

In order to further investigate the functional role of *Barhl1* in tumor development, *Math1-cre:Smom2^{F/+}* mice as a mouse model for Sonic hedgehog-associated medulloblastomas were used (Schüller *et al.*, 2008). To characterize *Barhl1* expression during development and in Sonic hedgehog-driven mouse medulloblastomas, in situ hybridizations for *Barhl1* on *WT* and *Math1-cre:Smom2^{F/+}* mice were performed. At postnatal day 7 (P7) *Barhl1* was strongly expressed in cerebellar granule neurons (Figure 11A). Granule neuron precursors were labeled intensely throughout the external granule cell layer of the entire cerebellum, but *Barhl1* expression was discontinuous in mature granule neurons of the internal granule cell layer (IGL). *Barhl1* expression in the IGL was seen in cerebellar lobes II-V and X and to some extent in lobe VI, while

it was absent in lobes VII, VIII and IX (Figure 11A). In medulloblastomas from *Math1-cre:Smom2^{F/+}* mice, *Barhl1* expression was strongly present in the tumor tissue, and a weaker expression was seen in granule neurons of the internal granule cell layer (Figure 11B). To confirm these findings, real-time RT-PCR was used to quantify *Barhl1* expression (Figure 11C). In agreement with the in situ experiments, *Barhl1* expression levels were about 10 times higher during cerebellar development (P7) in comparison to adult cerebellum (P30), and high expression was found in medulloblastomas from *Math1-cre:Smom2^{F/+}* mice.

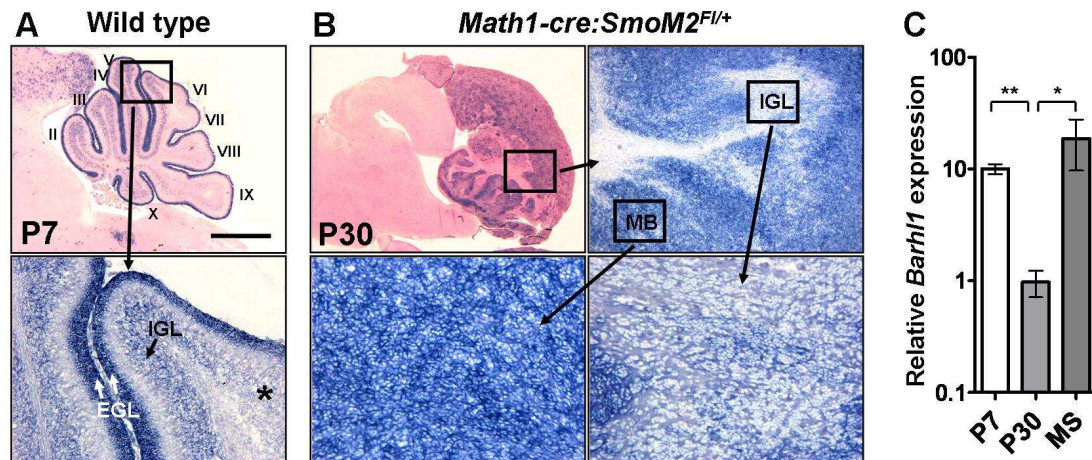


Figure 11: *Barhl1* is strongly expressed in the granule cell lineage and in tumors from *Math1-cre:Smom2^{F/+}* mice. **(A)** Sagittal sections from P7 wild type mice display strong expression of *Barhl1* in cerebellar granule neurons. While granule neuron precursors are labeled throughout the EGL of the entire cerebellum, *Barhl1* expression in mature granule neurons of the IGL is restricted to lobes II-V and X (see high power image with asterisk indicating *Barhl1*-negative granule neurons). **(B)** Sagittal cerebellar sections from *Math1-cre:Smom2^{F/+}* mice. Top left: H&E staining of a characteristic medulloblastoma in a *Math1-cre:Smom2^{F/+}* mouse. Top right: In situ hybridization for *Barhl1* in the cerebellum of a *Math1Cre:Smom2^{F/+}* mouse with strong expression in tumor tissue (lower left) and weak expression in IGL tissue (lower right). **(C)** Relative quantification of *Barhl1* expression using real-time RT-PCR with results normalized to *B2m*. *Barhl1* expression levels were significantly higher in cerebella on P7 and in medulloblastomas from *Math1-cre:Smom2^{F/+}* (MS) mice as compared to adult cerebella (P30, $p=0.002$ and $p=0.05$ respectively). EGL, External granule cell layer; IGL, Internal granule cell layer; MB, Medulloblastoma. One asterisk: $p\leq 0.05$, two asterisks: $p\leq 0.01$. Scale bar is 1 mm and 100 μm for A, 1.5 mm for the H&E stain, 200 μm for the *Barhl1* low power and 50 μm for the *Barhl1* high power images in B.

3.3. *Barhl1* *in vivo*

3.3.1. Deletion of *Barhl1* in mouse medulloblastoma

In order to investigate the functional role of *Barhl1* for the development and progression of medulloblastoma, *Barhl1*^{+/-}*Math1-cre:Smom2*^{F/+} and *Barhl1*^{-/-}*Math1-cre:Smom2*^{F/+} mice were generated. Similar to the previously described *Math1-cre:Smom2*^{F/+} mice (Schüller *et al.*, 2007), all generated *Barhl1*^{+/-}*Math1-cre:Smom2*^{F/+} and *Barhl1*^{-/-}*Math1-cre:Smom2*^{F/+} mice developed medulloblastomas. As seen by H&E staining, all three genotypes displayed a similar morphology with tumors composed of small round blue tumor cells in high density (Figure 12A). While *Barhl1* expression was strongly present in *Math1-cre:Smom2*^{F/+} mice, *Barhl1* levels were significantly decreased in *Barhl1*^{+/-}*Math1-cre:Smom2*^{F/+} mice (p=0.029) and were not detectable in *Barhl1*^{-/-}*Math1-cre:Smom2*^{F/+} mice (Figure 12B). To elucidate whether *Barhl1* expression in medulloblastoma has an impact on the survival of the mice, Kaplan-Meier curves of *Math1-cre:Smom2*^{F/+} mice (n=51), *Barhl1*^{+/-}*Math1-cre:Smom2*^{F/+} mice (n=46) and *Barhl1*^{-/-}*Math1-cre:Smom2*^{F/+} mice (n=12, Figure 12C) were established. Deletion of *Barhl1* resulted in a significantly decreased survival of *Barhl1*^{+/-}*Math1-cre:Smom2*^{F/+} and *Barhl1*^{-/-}*Math1-cre:Smom2*^{F/+} mice in comparison to *Math1-cre:Smom2*^{F/+} mice (p=0.003 and p=0.002, respectively).

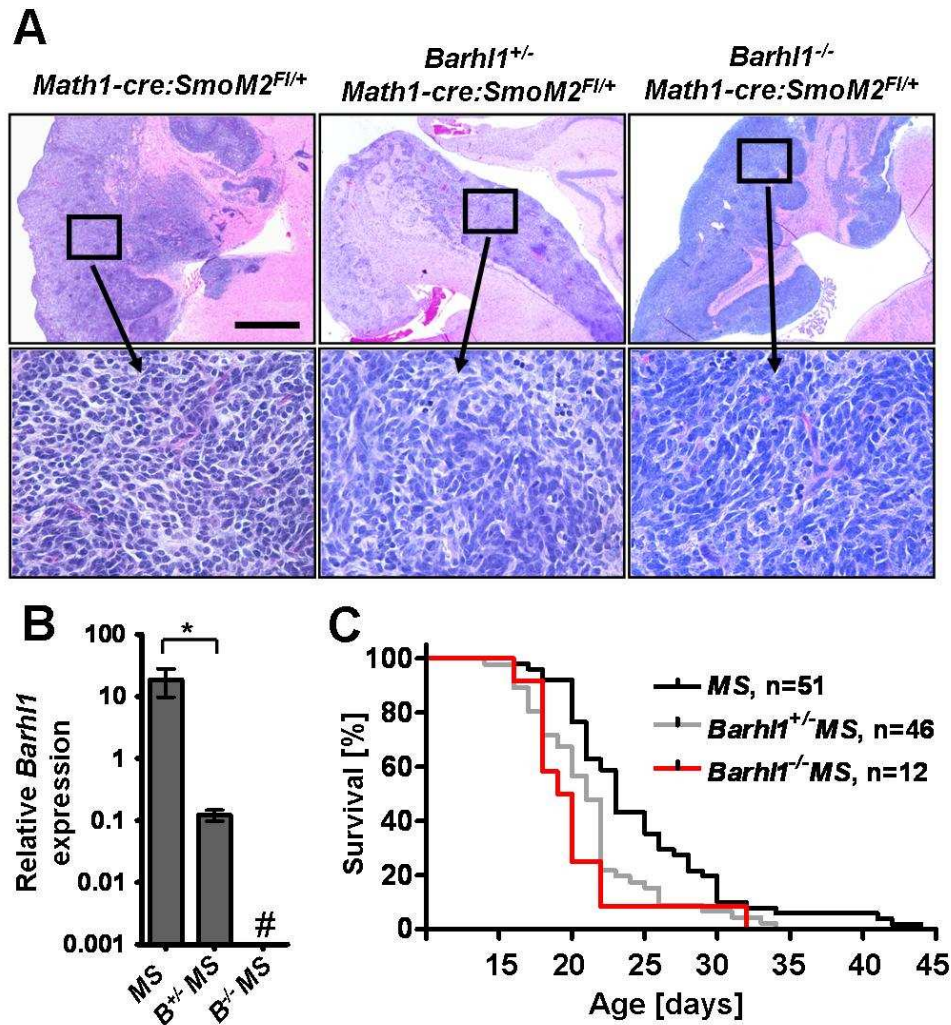


Figure 12: Deletion of *Barhl1* in *Math1-cre:Smom2^{F/+}* mice. (A) H&E staining of sagittal sections from medulloblastoma showed a similar morphology in *Math1-cre:Smom2^{F/+}*, *Barhl1^{+/-}Math1-cre:Smom2^{F/+}* and *Barhl1^{-/-}Math1-cre:Smom2^{F/+}* mice. High magnifications revealed small round blue tumor cells in high density. **(B)** *Barhl1* expression was analyzed using real-time RT-PCR. Target gene level was normalized to *B2m* mRNA. *Barhl1* levels were significantly decreased in *Barhl1^{+/-}Math1-cre:Smom2^{F/+}* (*B^{+/-}MS*) mice compared to *Math1-cre:Smom2^{F/+}* (*MS*) mice ($p=0.029$) and were not detectable in *Barhl1^{-/-}Math1-cre:Smom2^{F/+}* (*B^{-/-}MS*) mice. Hashmark indicates no detectable *Barhl1* expression. Asterisk: $p\leq 0.05$ **(C)** Survival curves for *Math1-cre:Smom2^{F/+}* (*MS*) mice ($n=51$), *Barhl1^{+/-}Math1-cre:Smom2^{F/+}* mice (*Barhl1^{+/-}MS*, $n=46$) and *Barhl1^{-/-}Math1-cre:Smom2^{F/+}* mice (*Barhl1^{-/-}MS*, $n=12$). Deletion of *Barhl1* resulted in a significantly decreased survival of *Barhl1^{+/-}Math1-cre:Smom2^{F/+}* mice and *Barhl1^{-/-}Math1-cre:Smom2^{F/+}* mice in comparison to *Math1-cre:Smom2^{F/+}* mice ($p=0.003$ and $p=0.002$ respectively). Scale bar is 1 mm for low power images and 50 μ m for high power images.

3.3.2. Immunohistochemical characterization of mouse medulloblastoma

To find out why *Barhl1* deletion resulted in a worse prognosis, *Math1-cre:Smom2^{F/+}*, *Barhl1^{+/-}Math1-cre:Smom2^{F/+}* and *Barhl1^{-/-}Math1-cre:Smom2^{F/+}* mice were further analyzed by immunohistochemistry. As expected, Cre recombinase expression was strong in all three genotypes with a large majority of tumor cells being stained (Figure 14). NeuN, a marker for neuronal differentiation, is expressed in mature granule neurons of the internal granule cell layer (Weyer and Schilling, 2003), but also in medulloblastoma (Eberhart *et al.*, 2001). Interestingly, *Math1-cre:Smom2^{F/+}*-derived medulloblastoma cells exhibited a strong expression of NeuN, but significantly fewer NeuN-positive cells were detectable in tumors from *Barhl1^{+/-}Math1-cre:Smom2^{F/+}* ($p=0.004$) and *Barhl1^{-/-}Math1-cre:Smom2^{F/+}* mice ($p=0.012$, Figure 13A). Similarly, expression of Zic, a marker for granule neuron differentiation and medulloblastoma (Yokota *et al.*, 1996) was significantly reduced in *Barhl1^{+/-}Math1-cre:Smom2^{F/+}* ($p=0.034$) and *Barhl1^{-/-}Math1-cre:Smom2^{F/+}* mice ($p=0.016$, Figure 13A). While Olig2 and Sox2, both of which label multipotent precursors (Schüller *et al.*, 2008; Sutter *et al.* 2010), were found to be similarly expressed in all three genotypes (Figure 14), Synaptophysin and MAP2, as additional markers for neuronal differentiation, appeared to be more weakly expressed in *Barhl1^{+/-}Math1-cre:Smom2^{F/+}* and *Barhl1^{-/-}Math1-cre:Smom2^{F/+}* mice than in *Math1-cre:Smom2^{F/+}* mice (Figure 14). In contrast, the percentage of phosphorylated Histone H3 (pHH3) positive tumor cells was significantly increased in *Barhl1^{-/-}Math1-cre:Smom2^{F/+}* mice in comparison to *Barhl1^{+/-}Math1-cre:Smom2^{F/+}* mice ($p=0.019$) and *Math1-cre:Smom2^{F/+}* mice ($p=0.012$). Likewise, *Barhl1^{+/-}Math1-cre:Smom2^{F/+}* mice showed an elevated fraction of pHH3-positive tumor cells when compared to *Math1-cre:Smom2^{F/+}* mice ($p=0.045$). Furthermore, Western Blot analysis showed that protein levels of cleaved caspase-3, a marker for apoptosis, were significantly reduced in *Barhl1^{-/-}Math1-cre:Smom2^{F/+}* mice when compared to *Math1-cre:Smom2^{F/+}* mice ($p=0.036$, Figure 13B), and this may indicate some pro-apoptotic effect in medulloblastoma. Hence, medulloblastomas from *Barhl1^{+/-}Math1-cre:Smom2^{F/+}* and *Barhl1^{-/-}Math1-cre:Smom2^{F/+}* mice were characterized by a significantly decreased differentiation of tumor cells.

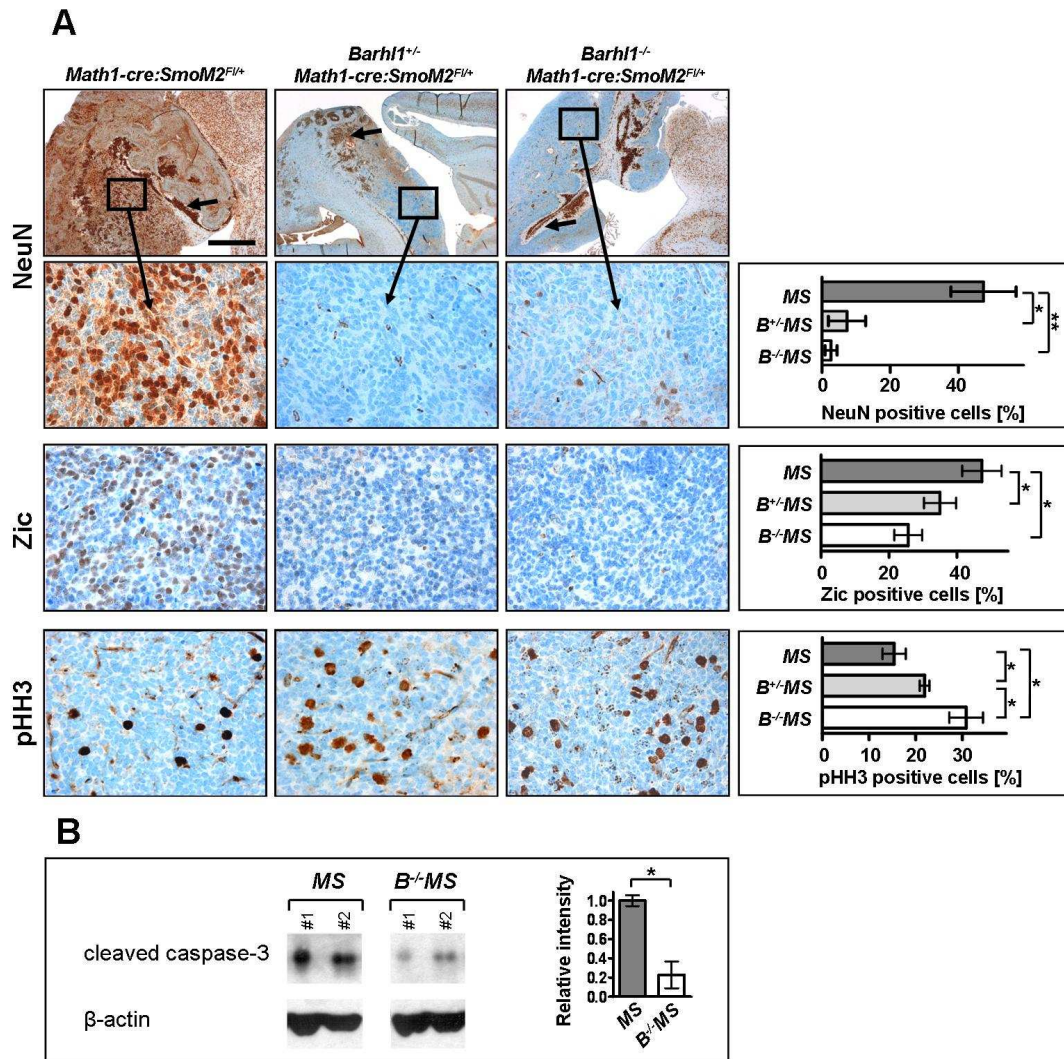


Figure 13: Immunohistochemical characterization of mouse medulloblastoma. (A) Immunostaining for NeuN, Zic and phosphorylated Histone H3 (pHH3). Scale bar is 1mm for low power images and 50 μ m for high power images. Immunostaining for NeuN: Arrows point at strongly stained mature granule neurons in the internal granule cell layer (IGL). Strong NeuN expression was also found in tumor cells from *Math1-cre:SmO2^{Fl/+}* mice, but only marginal expression was seen in tumors from *Barhl1^{+/-}Math1-cre:SmO2^{Fl/+}* and *Barhl1^{-/-}Math1-cre:SmO2^{Fl/+}* mice. The percentage of NeuN positive tumor cells was significantly reduced in *Barhl1^{+/-}Math1-cre:SmO2^{Fl/+}* (*B^{+/-}MS*) mice ($p=0.012$) and *Barhl1^{-/-}Math1-cre:SmO2^{Fl/+}* (*B^{-/-}MS*) mice ($p=0.004$) in comparison to *Math1-cre:SmO2^{Fl/+}* (*MS*) mice. Immunostaining for Zic: The percentage of Zic positive tumor cells was significantly reduced in *B^{+/-}MS* mice ($p=0.034$) and *B^{-/-}MS* mice ($p=0.016$) compared to *MS* mice. Immunostaining for pHH3: The percentage of pHH3-positive tumor cells was significantly increased in *B^{-/-}MS* mice in comparison to *B^{+/-}MS* mice ($p=0.019$) and *MS* mice ($p=0.012$). *B^{+/-}MS* mice showed increased pHH3-positive tumor cells when compared to *MS* mice ($p=0.045$).

(B) Western Blot for cleaved caspase-3. Protein levels of cleaved caspase-3 were significantly reduced in *Barhl1*^{-/-}*Math1-cre:Smom2*^{F/+} mice in comparison to *Math1-cre:Smom2*^{F/+} mice (p=0.036). One asterisk: p≤0.05, two asterisks: p≤0.01.

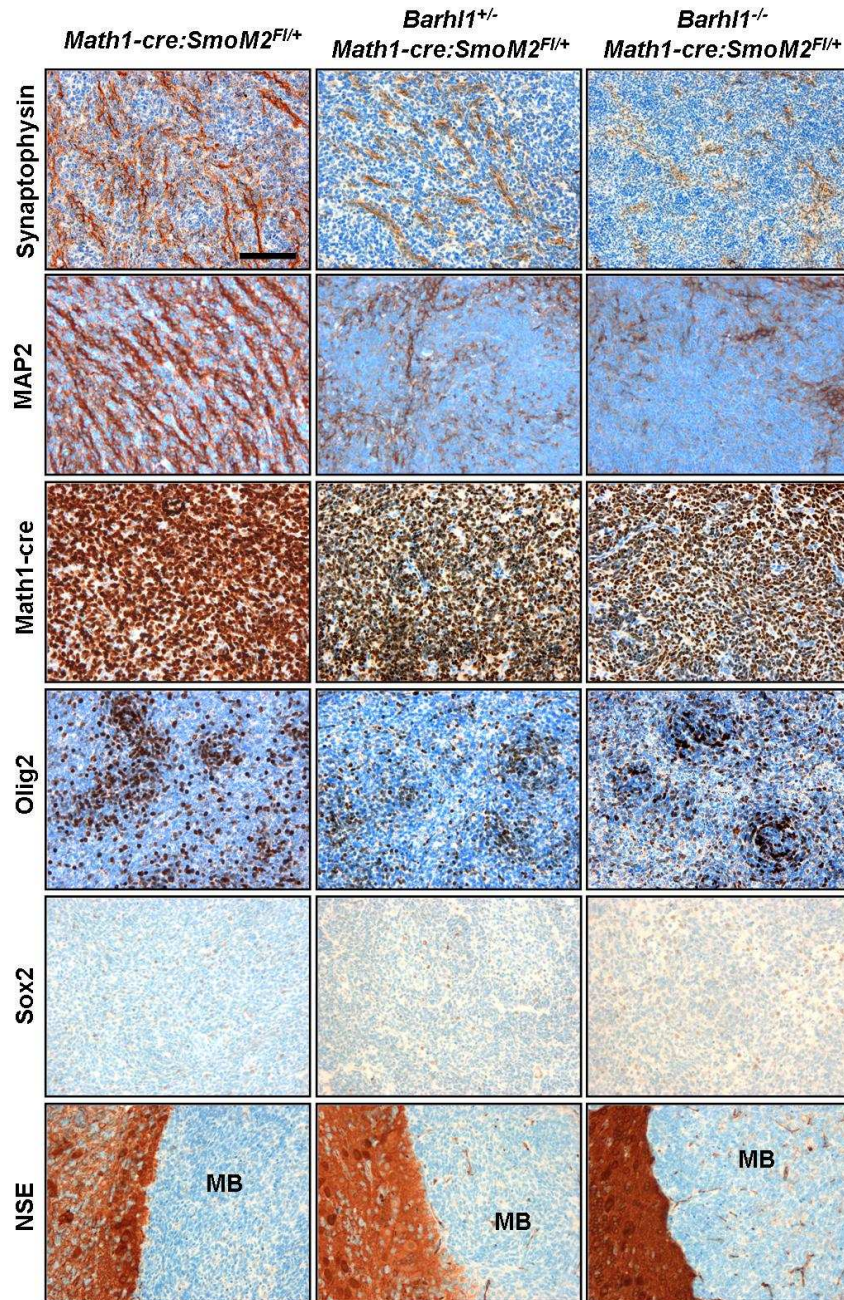


Figure 14: Immunohistochemical characterization of mouse medulloblastoma. Strong Synaptophysin expression was found in tumor cells from *Math1-cre:Smom2*^{F/+} mice, but only weak expression was seen in tumors from *Barhl1*^{+/-} *Math1-cre:Smom2*^{F/+} and *Barhl1*^{-/-} *Math1-cre:Smom2*^{F/+} mice. MAP2 displayed a similar pattern with robust staining in *Math1-cre:Smom2*^{F/+} mice and weak staining in *Barhl1*^{+/-} *Math1-*

cre:SmOM2^{F/+} and *Barhl1^{-/-} Math1-cre: SmOM2^{F/+}* mice. Cre recombinase expression was strong in all three genotypes with the large majority of tumor cells being stained. Expression of Math1-cre, Olig2 and Sox2 was similar in all tumor genotypes. Differentiated cells of the normal cerebellum exhibited strong NSE staining, but all medulloblastomas (MB) were NSE negative. Scale bar is 50 μ m for all images.

3.4. BARHL1 expression in human medulloblastomas and patients' survival

Having observed an important impact of *Barhl1* on the differentiation and prognosis of murine medulloblastoma, the next intention was to analyze the survival of patients with respect to *BARHL1* expression in human medulloblastoma. When separating the patients into two groups by using the median of relative *BARHL1* expression in medulloblastoma, statistically significant differences in survival were not seen (data not shown). However, the 13 patients exhibiting the highest relative *BARHL1* expression values (high *BARHL1*) were found to have a significantly better prognosis than the rest of the group (low *BARHL1*, n=31, p=0.049, Figure 15). In particular, after 5 years of follow-up, none of the high *BARHL1* cases had died, whereas the survival rate of patients with low *BARHL1* medulloblastomas was only 0.59 (Figure 15).

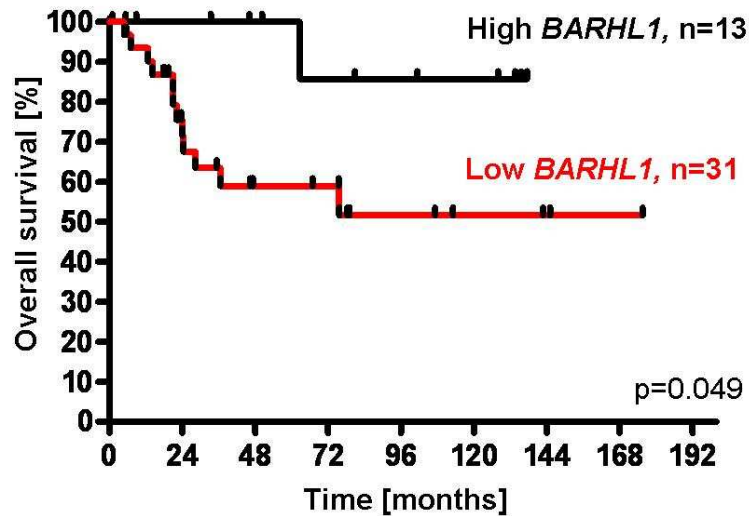


Figure 15: Kaplan Meier analysis of patients with medulloblastoma that express high or low levels of *BARHL1*. The 13 patients exhibiting the highest relative *BARHL1* expression values (high *BARHL1*) were compared to the rest of the group (low *BARHL1*, n=31). High levels of *BARHL1* were significantly correlated with a better prognosis ($p=0.049$).

To validate the prognostic value of *BARHL1* expression in a different set of medulloblastoma cases, the microarray expression data from an Amsterdam series of medulloblastoma patients were re-analyzed (Kool *et al.*, 2008) and Kaplan Meier curves with respect to *BARHL1* expression were established. To apply a similar threshold for *BARHL1* expression, at first an expression cut-off at third quartile was used to divide the Amsterdam series in high and low *BARHL1* cases. However, the 13 high *BARHL1* cases only tended to have a better survival than the low *BARHL1* cases, but statistical significance was not reached (n=36, $p=0.357$, Figure 16A). Nevertheless, a significantly prolonged overall survival was found after splitting the series into 41 patients with high *BARHL1* expression and 8 patients with low *BARHL1* expression ($p<0.001$, Figure 16B).

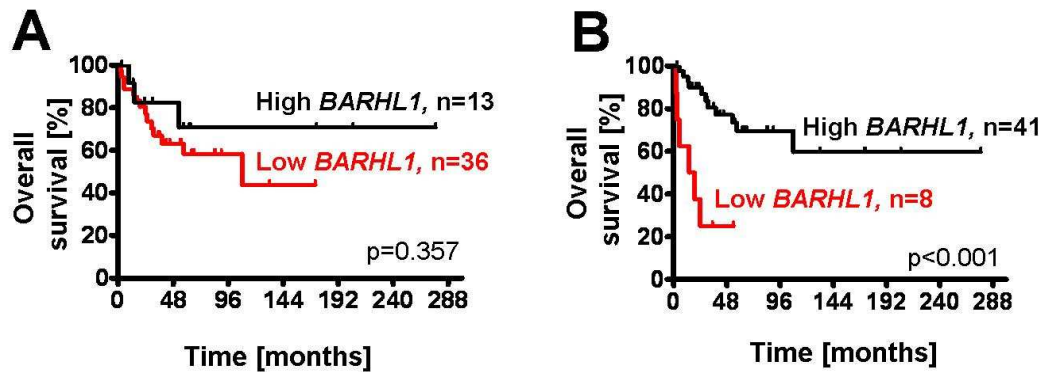


Figure 16: *BARHL1* expression and survival in a different set of medulloblastoma cases (Kool *et al.*, 2008). **(A)** Applying a similar threshold than in our patient group (expression cut-off at third quartile) shows a trend for favorable survival in the high *BARHL1* group (n=13) when compared to the rest of the group (low *BARHL1*, n=36, $p=0.357$). **(B)** A significantly prolonged overall survival was found in the 41 patients showing high *BARHL1* expression levels when compared to the remaining patients (low *BARHL1*, $p < 0.001$).

To see whether *BARHL1* also correlated with differentiation markers in human medulloblastoma, again the microarray expression data of 62 medulloblastoma samples from the Amsterdam series were re-analyzed. Expression levels of *NEUN* and *ZIC1* were significantly increased in the 50 medulloblastoma cases expressing *BARHL1* when compared to the 12 medulloblastoma samples with no detectable *BARHL1* expression ($p=0.001$ and $p=0.021$ respectively, see Figure 17A, B). Moreover, *MAP2* expression levels were found to be significantly correlated with *BARHL1* expression levels ($p < 0.001$, data not shown). These findings suggest that the effects of *BARHL1* were similar in mouse and human medulloblastoma, with loss or reduced *BARHL1* expression being associated with decreased differentiation of the tumor cells and a worse prognosis of mice and patients.

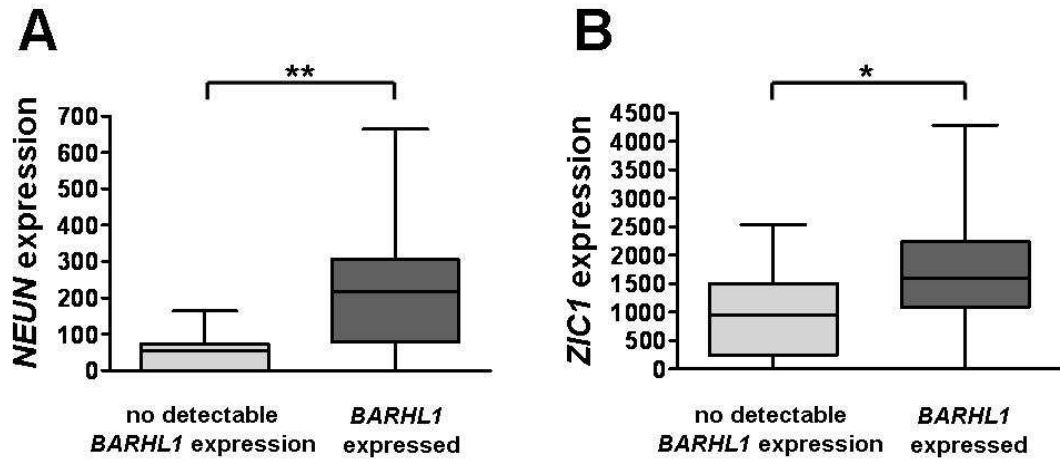


Figure 17: (A, B) Expression of differentiation markers with respect to *BARHL1* expression in the set of medulloblastoma cases from Kool *et al.* 2008. Expression levels of *NEUN* and *ZIC1* were significantly increased in the 50 medulloblastoma cases expressing *BARHL1* when compared to the 12 medulloblastoma samples with no detectable *BARHL1* expression (p=0.001 and p=0.021 respectively). One asterisk: p≤0.05, two asterisks: p≤0.01.

4. Discussion

Barhl1 is known to play a key role in cerebellar development having influence on migration and survival of granule neuron precursors (Li *et al.*, 2004). I observed that *Barhl1* expression was maintained in mature granule neurons of several anterior lobes of the cerebellum as well as in lobe X (Figure 11A). While expression of *Barhl1* in mature granule neurons per se was confirmed by lacZ expression in *Barhl1*^{-/-} mice (Li *et al.*, 2004), the regional specificity of *Barhl1* expression in the cerebellum has not yet been functionally analyzed. Interestingly, this expression pattern correlates well with the expression of *Gli1* and *En1* transcription factors, both of which are known to have crucial functions during cerebellar development (Millen *et al.*, 1995; Corrales *et al.*, 2004). While it is tempting to speculate on the functional role of *Barhl1* itself with respect to anteroposterior patterning, it appears possible that *Barhl1* functions in cooperation with the above mentioned genes.

I further report that *Barhl1* is expressed in medulloblastoma arising in *Math1-cre:Smom2*^{F/+} mice as well as in the majority of human medulloblastoma samples. Interestingly, loss of *Barhl1* in *Math1-cre:Smom2*^{F/+} derived medulloblastomas resulted in a down-regulation of neuronal differentiation markers, whereas mitotic activity of these cells was increased (Figure 13). Hence, apart from its role during normal cerebellar development, *Barhl1* might play important roles for cell differentiation in medulloblastoma. Moreover, deletion of *Barhl1* in *Math1-cre:Smom2*^{F/+} mice led to a significantly decreased survival of these mice. Similarly, patients with low *BARHL1* expression had a significantly worse prognosis and died earlier. The observation that loss of *Barhl1* causes migration deficits in neurons of *Barhl1* null mice (Li *et al.*, 2004), extenuates the possibility that unfavorable survival of patients with medulloblastoma with low levels of *Barhl1* expression might be due to enhanced migration or infiltration of medulloblastoma cells. I therefore suggest that the underlying mechanisms leading to a worse prognosis of patients and mice carrying tumors with low or no *BARHL1* expression are mainly decreased differentiation and increased proliferation of medulloblastoma cells.

A recent study found medulloblastoma to comprise 5 distinct molecular variants (Kool *et al.*, 2008). Besides the SHH-associated tumors, the WNT group and three other, not yet well characterized groups have been described. While the

used mouse model highlights the role of *Barhl1* in Shh-associated medulloblastomas, the functional impact of *Barhl1* on tumors belonging to other molecular subgroups appears hard to investigate, mainly due to the lack of appropriate mouse models. Interestingly enough, of the 13 medulloblastoma samples exhibiting the highest *BARHL1* expression values in our own series, 4 samples showed a desmoplastic histology which is often associated with SHH-associated medulloblastomas and one case carried a *CTNNB1* mutation, a criterion for the WNT-associated variant (Kool *et al.*, 2008). However, both desmoplastic histology and *CTNNB1* mutations were also found in tumors with low *BARHL1* expression. In line with this, expression of *BARHL1* was similar in desmoplastic and in classic medulloblastomas (Figure 1C), suggesting an important role of *Barhl1* for several, if not all medulloblastoma subtypes and indicating that the mechanisms revealed by *Barhl1* loss in *Math1-cre:SmoM2^{F/+}* mice might be applied to all medulloblastoma subtypes.

Barhl1 belongs to a family of homeodomain transcription factors which also includes the homologue *Barhl2*. Although these proteins are known to display distinct expression patterns in the nervous system, yet overlapping expression was found in granule neuron precursors of the cerebellum (Bulfone *et al.*, 2000; Li *et al.*, 2002; Mo *et al.*, 2004). Moreover, *Barhl1* and *Barhl2* can transactivate the *Barhl1* promoter (Chellappa *et al.*, 2008). This could not only point towards a close interaction between *Barhl1* and *Barhl2* in granule neuron precursors but also to some compensating mechanisms in a *Barhl1*-null situation. However, I did not find any upregulation of *Barhl2* expression in medulloblastomas from *Barhl1^{+/-}Math1-cre:SmoM2^{F/+}* and *Barhl1^{-/-}Math1-cre:SmoM2^{F/+}* mice. Neither was *Barhl2* upregulated in *Barhl1^{-/-}* and *Barhl1^{+/-}* mice. Therefore, the function of *Barhl2* in medulloblastoma pathology and normal granule cell development seems to be distinct from *Barhl1* functions and effects of *Barhl1* loss were neither mediated, nor extenuated by *Barhl2*. A statistically significant difference in survival with respect to *BARHL1* expression was found in our group of 44 patients. However, re-analysis of the microarray expression data from the Amsterdam series of medulloblastoma patients (Kool *et al.*, 2008) did not confirm these results when using the same cutoff for *BARHL1* expression as a prognostic indicator. This reinforces the fact that molecular markers relying on percentile rankings are not suitable for human clinical trials. Although *BARHL1* seems biologically important in medulloblastomas, its prognostic value still has

to be defined, ideally prospectively in a large homogenously treated cohort of patients.

Similar to Barhl1, several other genes are known to be associated with a favorable prognosis in medulloblastoma (Pomeroy *et al.*, 2002). Among them, TRKC, the receptor for Neurotrophin-3 (NT-3), is well described (Segal *et al.*, 1994). Interestingly, its ligand, Nt-3, was suggested to be a major downstream gene of Barhl1 during cerebellar development (Li *et al.*, 2004). Further understanding of the molecular interactions of BARHL1 and its partners will be promising to find specific therapeutic strategies for medulloblastoma treatment in the future.

5. Summary

5.1. Summary

Medulloblastoma is the most common malignant brain tumor in childhood, and development of targeted therapies is highly desired. While the molecular mechanisms of malignant transformation are not fully understood, it is known that medulloblastoma may arise from cerebellar granule neuron precursors. The homeodomain transcription factor *Barhl1* is known to regulate migration and survival of granule cell precursors, but its functional role in medulloblastoma is unknown. It is shown here that expression of *BARHL1* is significantly upregulated during human cerebellar development and in human medulloblastoma samples as compared to normal adult cerebellum. High levels of *Barhl1* expression were detected in medulloblastomas of *Math1-cre:Smom2^{F/+}* mice, an established mouse model for Sonic hedgehog-associated medulloblastomas. To investigate *Barhl1* function *in vivo* during tumor development, *Barhl1^{-/-}Math1-cre:Smom2^{F/+}* and *Barhl1^{+/-}Math1-cre:Smom2^{F/+}* mice were generated. Interestingly, tumors that developed in these mice displayed increased mitotic activity and decreased neuronal differentiation. Moreover, survival of these mice was significantly decreased. Similarly, low expression of *BARHL1* in human medulloblastoma cases was associated with a less favorable prognosis for the patients. These results suggest that expression of *Barhl1* decelerates tumor growth both in human and murine medulloblastoma and should be further investigated with respect to potential implications for individualized therapeutic strategies.

5.2. Zusammenfassung

Das Medulloblastom ist der häufigste maligne Hirntumor des Kindesalters, und die Entwicklung von zielgerichteten, nebenwirkungsarmen Therapiestrategien hat oberste Priorität. Die molekularen Mechanismen der malignen Transformation dieses Tumors sind noch nicht bis ins Letzte verstanden, jedoch ist bekannt, dass Medulloblastome von Körnerzellvorläufern abstammen können. *Barhl1* ist einer der Transkriptionsfaktoren, die das Überleben und die Migration von Körnerzellvorläufern steuern, jedoch ist die Funktion, die *Barhl1* im Medulloblastom hat, noch unbekannt. Diese Arbeit zeigt, dass die Expression von *BARHL1* während der Entwicklungsphase des menschlichen Kleinhirns und in humanen Medulloblastomen im Vergleich zu Kleinhirnen von Erwachsenen signifikant hochreguliert ist. Hohe *Barhl1* Expressionslevel wurden zudem in Medulloblastomen von *Math1-cre:SmoM2^{Fl/+}* Mäusen gefunden, welche ein bewährtes Mausmodell für Sonic hedgehog-assoziierte Medulloblastome darstellen, die von cerebellären Körnerzellvorläufern abstammen. Um die Funktion von *Barhl1 in vivo* während der Entwicklung und des Wachstums von Medulloblastomen zu untersuchen, wurden *Barhl1^{-/-}Math1-cre:SmoM2^{Fl/+}* und *Barhl1^{+/-}Math1-cre:SmoM2^{Fl/+}* Mäuse generiert. Interessanterweise zeigten Tumoren, die in diesen Mäusen entstanden, eine vermehrte mitotische Aktivität und eine verminderte neuronale Differenzierung. Zudem war das Überleben dieser Mäuse im Vergleich zu dem von *Math1-cre:SmoM2^{Fl/+}* Mäusen signifikant verkürzt. Im Einklang mit diesen Ergebnissen zeigten Patienten, deren Medulloblastom eine niedrige *BARHL1* Expression aufwies, eine schlechtere Prognose als Patienten, deren Tumoren eine höhere *BARHL1* Expression aufwiesen. Diese Ergebnisse deuten darauf hin, dass die Expression von *Barhl1* das Tumorwachstum in murinen und humanen Medulloblastomen verlangsamt. Deswegen sollte *BARHL1* im Hinblick auf potentielle Anwendungen für individualisierte therapeutische Strategien weiter untersucht werden.

6. References

Alston RD, Newton R, Kelsey A, Newbould MJ, Birch JM, Lawson B, McNally RJ (2003). Childhood medulloblastoma in northwest England 1954 to 1997: incidence and survival. *Dev Med Child Neurol* **45**: 308-14.

Bulfone A, Menguzzato E, Broccoli V, Marchitello A, Gattuso C, Mariani M, Consalez GG, Martinez S, Ballabio A, Banfi S (2000). Barhl1, a gene belonging to a new subfamily of mammalian homeobox genes, is expressed in migrating neurons of the CNS. *Hum Mol Genet* **9**: 1443-52.

Chellappa R, Li S, Pauley S, Jahan I, Jin K, Xiang M (2008). Barhl1 regulatory sequences required for cell-specific gene expression and autoregulation in the inner ear and central nervous system. *Mol Cell Biol* **28**: 1905-14.

Cho YJ, Tsherniak A, Tamayo P, Santagata S, Ligon A, Greulich H, Berhoukim R, Amani V, Goumnerova L, Eberhart CG, Lau CC, Olson JM, Gilbertson RJ, Gajjar A, Delattre O, Kool M, Ligon K, Meyerson M, Mesirov JP, Pomeroy SL (2011). Integrative Genomic Analysis of Medulloblastoma Identifies a Molecular Subgroup That Drives Poor Clinical Outcome. *J Clin Oncol*. **29**:1424-30

Corrales JD, Rocco GL, Blaess S, Guo Q, Joyner AL (2004). Spatial pattern of sonic hedgehog signaling through Gli genes during cerebellum development. *Development* **131**: 5581-90.

Crawford JR, MacDonald TJ, Packer RJ (2007). Medulloblastoma in childhood: new biological advances. *Lancet Neurol* **6**: 1073-85.

Eberhart CG, Kaufman WE, Tihan T, Burger PC (2001). Apoptosis, neuronal maturation, and neurotrophin expression within medulloblastoma nodules. *J Neuropathol Exp Neurol* **60**: 462-9.

Evans AE, Jenkin RD, Spoto R, Ortega JA, Wilson CB, Wara W, Ertel IJ, Kramer S, Chang CH, Leikin SL, Hammond GD (1990). The treatment of medulloblastoma. Results of a prospective randomized trial of radiation therapy with and without CCNU, vincristine, and prednisone. *J Neurosurg* **72**: 572-82.

Gibson P, Tong Y, Robinson G, Thompson MC, Currie DS, Eden C, Kranenburg TA, Hogg T, Poppleton H, Martin J, Finkelstein D, Pounds S, Weiss A, Patay Z, Scoggins M, Ogg R, Pei Y, Yang ZJ, Brun S, Lee Y, Zindy F, Lindsey JC, Taketo MM, Boop FA, Sanford RA, Gajjar A, Clifford SC, Roussel MF, McKinnon PJ, Gutmann DH, Ellison DW, Wechsler-Reya R, Gilbertson RJ (2010). Subtypes of medulloblastoma have distinct developmental origins. *Nature* **468**: 1095-9.

Gilbertson RJ (2004). Medulloblastoma: signalling a change in treatment. *Lancet Oncol* **5**: 209-18.

Gjerris F, Agerlin N, Borgesen SE, Buhl L, Haase J, Klinken L, Mortensen AC, Olsen JH, Ovesen N, Reske-Nielsen E, Schmidt K (1998). Epidemiology and prognosis in children treated for intracranial tumours in Denmark 1960-1984. *Childs Nerv Syst* **14**: 302-11.

Hartmann W, Koch A, Brune H, Waha A, Schüller U, Dani I, Denkhaus D, Langmann W, Bode U, Wiestler OD, Schilling K, Pietsch T (2005). Insulin-like growth factor II is involved in the proliferation control of medulloblastoma and its cerebellar precursor cells. *Am J Pathol* **166**: 1153-62.

Heine VM, Rowitch DH (2009). Hedgehog signaling has a protective effect in glucocorticoid-induced mouse neonatal brain injury through an 11betaHSD2-dependent mechanism. *J Clin Invest* **119**: 267-77.

Hughes EN, Shillito J, Sallan SE, Loeffler JS, Cassady JR, Tarbell NJ (1988). Medulloblastoma at the joint center for radiation therapy between 1968 and 1984. The influence of radiation dose on the patterns of failure and survival. *Cancer* **61**: 1992-8.

Jeong J, Mao J, Tenzen T, Kottmann AH, McMahon AP (2004). Hedgehog signaling in the neural crest cells regulates the patterning and growth of facial primordia. *Genes Dev* **18**: 937-51.

Kleihues P, Sobin LH (2000). World Health Organization classification of tumors. *Cancer* **88**: 2887.

Kool M, Koster J, Bunt J, Hasselt NE, Lakeman A, van Sluis P, Troost D, Meeteren NS, Caron HN, Cloos J, Mrcic A, Ylstra B, Grajkowska W, Hartmann W, Pietsch T, Ellison D, Clifford SC, Versteeg R (2008). Integrated genomics identifies five medulloblastoma subtypes with distinct genetic profiles, pathway signatures and clinicopathological features. *PLoS One* **3**: e3088.

Kortmann RD, Kuhl J, Timmermann B, Mittler U, Urban C, Budach V, Richter E, Willich N, Flentje M, Berthold F, Slavc I, Wolff J, Meisner C, Wiestler O, Sorensen N, Warmuth-Metz M, Bamberg M (2000). Postoperative neoadjuvant chemotherapy before radiotherapy as compared to immediate radiotherapy followed by maintenance chemotherapy in the treatment of medulloblastoma in childhood: results of the German prospective randomized trial HIT '91. *Int J Radiat Oncol Biol Phys* **46**: 269-79.

Laughton SJ, Merchant TE, Sklar CA, Kun LE, Fouladi M, Broniscer A, Morris EB, Sanders RP, Krasin MJ, Shelso J, Xiong Z, Wallace D, Gajjar A (2008). Endocrine outcomes for children with embryonal brain tumors after risk-adapted craniospinal and conformal primary-site irradiation and high-dose chemotherapy with stem-cell rescue on the SJMB-96 trial. *J Clin Oncol* **26**: 1112-8.

Li S, Price SM, Cahill H, Ryugo DK, Shen MM, Xiang M (2002). Hearing loss caused by progressive degeneration of cochlear hair cells in mice deficient for the Barhl1 homeobox gene. *Development* **129**: 3523-32.

Li S, Qiu F, Xu A, Price SM, Xiang M (2004). Barhl1 regulates migration and survival of cerebellar granule cells by controlling expression of the neurotrophin-3 gene. *J Neurosci* **24**: 3104-14.

Louis DN, Ohgaki H, Wiestler OD, Cavenee WK, Burger PC, Jouvet A, Scheithauer BW, Kleihues P (2007). The 2007 WHO classification of tumours of the central nervous system. *Acta Neuropathol* **114**: 97-109.

Mao J, Ligon KL, Rakhlin EY, Thayer SP, Bronson RT, Rowitch D, McMahon AP (2006). A novel somatic mouse model to survey tumorigenic potential applied to the Hedgehog pathway. *Cancer Res* **66**: 10171-8.

Matei V, Pauley S, Kaing S, Rowitch D, Beisel KW, Morris K, Feng F, Jones K, Lee J, Fritsch B (2005). Smaller inner ear sensory epithelia in Neurog 1 null mice are related to earlier hair cell cycle exit. *Dev Dyn* **234**: 633-50.

Millen KJ, Hui CC, Joyner AL (1995). A role for En-2 and other murine homologues of Drosophila segment polarity genes in regulating positional information in the developing cerebellum. *Development* **121**: 3935-45.

Mo Z, Li S, Yang X, Xiang M (2004). Role of the Barhl2 homeobox gene in the specification of glycinergic amacrine cells. *Development* **131**: 1607-18.

Northcott PA, Korshunov A, Witt H, Hielscher T, Eberhart CG, Mack S, Bouffet E, Clifford SC, Hawkins CE, French P, Rutka JT, Pfister S, Taylor MD (2011). Medulloblastoma Comprises Four Distinct Molecular Variants. *J Clin Oncol*. **29**: 1408-14

Packer RJ, Gajjar A, Vezina G, Rorke-Adams L, Burger PC, Robertson PL, Bayer L, LaFond D, Donahue BR, Marymont MH, Muraszko K, Langston J, Spoto R (2006). Phase III study of craniospinal radiation therapy followed by adjuvant chemotherapy for newly diagnosed average-risk medulloblastoma. *J Clin Oncol* **24**: 4202-8.

Pomeroy SL, Tamayo P, Gaasenbeek M, Sturla LM, Angelo M, McLaughlin ME, Kim JY, Goumnerova LC, Black PM, Lau C, Allen JC, Zagzag D, Olson JM, Curran T, Wetmore C, Biegel JA, Poggio T, Mukherjee S, Rifkin R, Califano A, Stolovitzky G, Louis DN, Mesirov JP, Lander ES, Golub TR (2002). Prediction of central nervous system embryonal tumour outcome based on gene expression. *Nature* **415**: 436-42.

Rademaker-Lakhai JM, Crul M, Zuur L, Baas P, Beijnen JH, Simis YJ, van Zandwijk N, Schellens JH (2006). Relationship between cisplatin administration and the development of ototoxicity. *J Clin Oncol* **24**: 918-24.

Ris MD, Packer R, Goldwein J, Jones-Wallace D, Boyett JM (2001). Intellectual outcome after reduced-dose radiation therapy plus adjuvant chemotherapy for medulloblastoma: a Children's Cancer Group study. *J Clin Oncol* **19**: 3470-6.

Scales SJ, de Sauvage FJ (2009). Mechanisms of Hedgehog pathway activation in cancer and implications for therapy. *Trends Pharmacol Sci* **30**: 303-12.

Schüller U, Heine VM, Mao J, Kho AT, Dillon AK, Han YG, Huillard E, Sun T, Ligon AH, Qian Y, Ma Q, Alvarez-Buylla A, McMahon AP, Rowitch DH, Ligon KL (2008). Acquisition of granule neuron precursor identity is a critical determinant of progenitor cell competence to form Shh-induced medulloblastoma. *Cancer Cell* **14**: 123-34.

Schüller U, Zhao Q, Godinho SA, Heine VM, Medema RH, Pellman D, Rowitch DH (2007). Forkhead transcription factor FoxM1 regulates mitotic entry and prevents spindle defects in cerebellar granule neuron precursors. *Mol Cell Biol* **27**: 8259-70.

Segal RA, Goumnerova LC, Kwon YK, Stiles CD, Pomeroy SL (1994). Expression of the neurotrophin receptor TrkC is linked to a favorable outcome in medulloblastoma. *Proc Natl Acad Sci U S A* **91**: 12867-71.

Soriano P (1999). Generalized lacZ expression with the ROSA26 Cre reporter strain. *Nat Genet* **21**: 70-1.

Srinivas S, Watanabe T, Lin CS, Williams CM, Tanabe Y, Jessell TM, Costantini F (2001). Cre reporter strains produced by targeted insertion of EYFP and ECFP into the ROSA26 locus. *BMC Dev Biol* **1**: 4.

Sutter R, Shakhova O, Bhagat H, Behesti H, Sutter C, Penkar S, Santucci A, Bernays R, Heppner FL, Schüller U, Grotzer M, Moch H, Schraml P, Marino S (2010). Cerebellar stem cells act as medulloblastoma-initiating cells in a mouse model and a neural stem cell signature characterizes a subset of human medulloblastomas. *Oncogene* **29**: 1845-56.

Tait DM, Thornton-Jones H, Bloom HJ, Lemerle J, Morris-Jones P (1990). Adjuvant chemotherapy for medulloblastoma: the first multi-centre control trial of the International Society of Paediatric Oncology (SIOP I). *Eur J Cancer* **26**: 464-9.

Tarbell NJ, Loeffler JS, Silver B, Lynch E, Lavalley BL, Kupsky WJ, Scott RM, Sallan SE (1991). The change in patterns of relapse in medulloblastoma. *Cancer* **68**: 1600-4.

Taylor RE, Bailey CC, Robinson K, Weston CL, Ellison D, Ironside J, Lucraft H, Gilbertson R, Tait DM, Walker DA, Pizer BL, Imeson J, Lashford LS (2003). Results of a randomized study of preradiation chemotherapy versus radiotherapy alone for nonmetastatic medulloblastoma: The International Society of Paediatric Oncology/United Kingdom Children's Cancer Study Group PNET-3 Study. *J Clin Oncol* **21**: 1581-91.

Thorne RN, Pearson AD, Nicoll JA, Coakham HB, Oakhill A, Mott MG, Foreman NK (1994). Decline in incidence of medulloblastoma in children. *Cancer* **74**: 3240-4.

Weyer A, Schilling K (2003). Developmental and cell type-specific expression of the neuronal marker NeuN in the murine cerebellum. *J Neurosci Res* **73**: 400-9.

Xie J, Murone M, Luoh SM, Ryan A, Gu Q, Zhang C, Bonifas JM, Lam CW, Hynes M, Goddard A, Rosenthal A, Epstein EH, de Sauvage FJ (1998). Activating Smoothed mutations in sporadic basal-cell carcinoma. *Nature* **391**: 90-2.

Xu W, Janss A, Packer RJ, Phillips P, Goldwein J, Moshang T, Jr. (2004). Endocrine outcome in children with medulloblastoma treated with 18 Gy of craniospinal radiation therapy. *Neuro Oncol* **6**: 113-8.

Yokota N, Aruga J, Takai S, Yamada K, Hamazaki M, Iwase T, Sugimura H, Mikoshiba K (1996). Predominant expression of human zic in cerebellar granule cell lineage and medulloblastoma. *Cancer Res* **56**: 377-83.

7. Acknowledgements

Special thanks go to my supervisor PD Dr. med. Ulrich Schüller for giving me the opportunity to work on this interesting topic, for always taking the time to answer my questions, for his exceptional support and for a lot of fruitful and motivating discussions. Moreover, I like to thank the director of the Zentrum für Neuropathologie und Prionforschung, Prof. Dr. med. Dr. h. c. Hans Kretzschmar, for giving me the possibility to do my work at this institution. I am indebted to Michael Schmidt, Veronika Kaltenbrunn, Dagmar Metzger, Philipp Neumann, and Silvia Occhionero for excellent technical support and to Dr. Mehdi Shakarami and Dr. Stefanie Ohlemeyer for animal husbandry. I acknowledge Prof. Dr. Rosalind Segal for providing Zic antibodies and Dr. Shengguo Li and Prof. Dr. Mengqing Xiang for providing the *Barhl1*^{-/-} mice. I refer to Dr. Andreas Lorenz, PD Dr. Aurelia Peraud, Dr. André von Bueren, Prof. Dr. Jörg-Christian Tonn, Prof. Dr. Stefan Rutkowski and Prof. Dr. Jochen Herms for providing human tumor samples and clinical information. I thank PD Dr. Wolfgang Hartmann for help with the Western blot and Dr. Marcel Kool for providing his data for re-analysis. Additionally, I want to thank the Kind-Philipp-Stiftung für Leukämieforschung for financial support when presenting my results at the XVIIth International Congress of Neuropathology.